Archives of Toxicology (2019) 93:3549–3583
https://doi.org/10.1007/s00204-019-02611-6

IN VITRO SYSTEMS

Transcriptomic characterization of culture-associated changes in murine and human precision-cut tissue slices

Emilia Bigaeva[1] · Emilia Gore[1] · Eric Simon[2] · Matthias Zwick[2] · Anouk Oldenburger[3] · Koert P. de Jong[4] · Hendrik S. Hofker[5] · Marco Schlepütz[6] · Paul Nicklin[7] · Miriam Boersema[1] · Jörg F. Rippmann[3] · Peter Olinga[1]

Received: 24 July 2019 / Accepted: 5 November 2019 / Published online: 21 November 2019

Abstract

Our knowledge of complex pathological mechanisms underlying organ fibrosis is predominantly derived from animal studies. However, relevance of animal models for human disease is limited; therefore, an ex vivo model of human precision-cut tissue slices (PCTS) might become an indispensable tool in fibrosis research and drug development by bridging the animal–human translational gap. This study, presented as two parts, provides comprehensive characterization of the dynamic transcriptional changes in PCTS during culture by RNA sequencing. Part I investigates the differences in culture-induced responses in murine and human PCTS derived from healthy liver, kidney and gut. Part II delineates the molecular processes in cultured human PCTS generated from diseased liver, kidney and ileum. We demonstrated that culture was associated with extensive transcriptional changes and impacted PCTS in a universal way across the organs and two species by triggering an inflammatory response and fibrosis-related extracellular matrix (ECM) remodelling. All PCTS shared mRNA upregulation of IL-11 and ECM-degrading enzymes MMP3 and MMP10. Slice preparation and culturing activated numerous pathways across all PCTS, especially those involved in inflammation (IL-6, IL-8 and HMGB1 signalling) and tissue remodelling (osteoarthritis pathway and integrin signalling). Despite the converging effects of culture, PCTS display species-, organ- and pathology-specific differences in the regulation of genes and canonical pathways. The underlying pathology in human diseased PCTS endures and influences biological processes like cytokine release. Our study reinforces the use of PCTS as an ex vivo fibrosis model and supports future studies towards its validation as a preclinical tool for drug development.

Keywords Precision-cut tissue slices · Fibrosis · Inflammation · Human tissue · RNA sequencing · Ingenuity pathway analysis

Introduction

The idea of tissue slices has been around for almost a century (Warburg 1923; Krebs 1933). However, it was not until 1980, when Krumdieck et al. (1980) developed a tissue slicer that enabled cutting of thin slices with precise thickness, the tissue slice technique received renewed attention. Precision-cut tissue slices (PCTS) capture the complex organotypic three-dimensional cellular structure, as each slice retains all cell types present in their original tissue-matrix configuration (de Graaf et al. 2007).

PCTS model is a promising tool for pharmaceutical research and development: it could bridge the translational gap between in vitro and in vivo studies. Many drugs fail development, suggesting that conventional preclinical models lack translatability and predictiveness for human diseases. In turn, the PCTS model is versatile, as both rodent and human tissue, healthy and diseased, can be used to prepare slices. In contrast to in vivo studies, PCTS offer the possibility for simultaneous use of different organs from the same animal, as well as for evaluation of multiple experimental conditions at once since multiple slices can be prepared from one organ. The use of human tissue significantly

Emilia Bigaeva and Emilia Gore contributed equally to this work.

Jörg F. Rippmann and Peter Olinga share last authorship.

Electronic supplementary material The online version of this article (https://doi.org/10.1007/s00204-019-02611-6) contains supplementary material, which is available to authorized users.

✉ Peter Olinga
p.olinga@rug.nl

Extended author information available on the last page of the article

improves the clinical relevance of PCTS by eliminating the need of cross-species translation. Therefore, the PCTS model contributes to the substantial reduction of animal use in biomedical research.

PCTS are used for a wide range of applications due to the fact that slices can be prepared from virtually any solid organ [liver, kidney, heart and several tumor types (Bull et al. 2000; Parajuli and Doppler 2009; Luangmonkong et al. 2017; Stribos et al. 2017)] as well as from non-solid organs [intestine and lung (Wohlsen et al. 2001; de Kanter et al. 2005)]. The applications of PCTS evolved from studies of liver functions (Krumdieck et al. 1980) to the use in xenobiotic metabolism, transport and toxicity research (de Graaf et al. 2007; Li et al. 2016; Vatakuti et al. 2016). Slices can be used to study the ischemia/reperfusion damage ('t Hart et al. 2005; Lee et al. 2008) and uptake of nanoparticles as carriers for gene therapy agents (Osman et al. 2018). Recently, the application of PCTS was further extended to study the mechanism of fibrosis, which is characterized by the excess deposition of extracellular matrix. It has been shown that PCTS from different organs develop inflammatory and fibrogenic responses during culture, making PCTS a suitable model for fibrosis and analysing the effect of antifibrotic compounds (Kasper et al. 2004; Westra et al. 2014, 2016; Pham et al. 2015; Stribos et al. 2016; Alsafadi et al. 2017; Luangmonkong et al. 2017, 2018). Furthermore, PCTS generated from human diseased organs allow the investigation of fibrosis in situ, as we previously showed for human cirrhotic liver PCTS (Luangmonkong et al. 2017).

Despite the extensive applications of PCTS, its recognition is limited by the lack of validation and molecular characterization. As a step towards validation, we attempted to describe the transcriptional changes in PCTS during culture by deep sequencing. In the past decade, next-generation sequencing (NGS) revolutionized the fields of genetics and biology, providing highly sensitive measurement of whole transcriptomes. RNA-Seq, as one of NGS applications, enables high-throughput transcriptomic analysis of gene expression profiles at the tissue level (Metzker 2010) and can be applied to various species and sources of RNA/DNA. The main advantages of RNA-Seq include high detection sensitivity, accuracy, increased automation and relatively low cost (Yadav et al. 2014).

The present study provides a comprehensive characterization of the dynamic transcriptional changes in PCTS during culture, and is divided into two parts. In Part I, we performed total RNA sequencing of murine and human PCTS prepared from various healthy organs (liver, kidney and gut) to investigate species and organ differences in culture-induced responses. In Part II of this study, we characterized molecular processes that occur in human PCTS generated from diseased (fibrotic) tissues during culture, and performed in-depth comparative analysis of transcriptomic profiles of human diseased and healthy control PCTS. Particular emphasis was placed on inflammation- and fibrosis-associated processes in PCTS. The findings largely contribute to our understanding of molecular mechanisms involved in PCTS culture, laying the foundation for the future validation of PCTS as an ex vivo injury/fibrosis model and a preclinical tool for drug development.

Methods

Ethical statement

The animal experiments were approved by the Animal Ethics Committee of the University of Groningen (DEC 6416AA-001).

The use of human material was approved by the Medical Ethical Committee of the University Medical Centre Groningen (UMCG), according to Dutch legislation and the Code of Conduct for dealing responsibly with human tissue in the context of health research (www.federa.org), refraining the need of written consent for 'further use' of coded-anonymous human tissue.

Animal and human material

Adult, 8–10 weeks old, male C57BL/6 mice (De Centrale Dienst Proefdieren, UMCG, Groningen, The Netherlands) with an average weight of 28.9 g (± 1.1) were housed under standard conditions with free access to chow and water. Five different animals were used for each organ. Murine organs were harvested after a terminal procedure performed under isoflurane/O_2 anaesthesia and stored in ice-cold tissue preservation solution (University of Wisconsin (UW) for liver, kidney and lung, or supplemented Krebs–Henseleit buffer (KHB) for jejunum, ileum and colon).

Human tissue was obtained from surplus resected material from patients with varying underlying diseases (Table 1). Patient demographics are included in Table S1. The tissue from three to five patients was used for obtaining PCTS (biological replicates). Ice-cold UW and KHB were used for human material preservation until further use.

Preparation of precision-cut tissue slices (PCTS)

PCTS from mouse and human liver and intestine were prepared as previously described (de Graaf et al. 2010). Preparation of mouse and human kidney slices was described by Stribos et al. (Stribos et al. 2016, 2017), while lung slices were prepared as described by Ruigrok et al. (2017). Slices were obtained with Krumdieck slicer filled with ice-cold KHB supplemented with 25 mM D-glucose (Merck, Darmstadt, Germany), 25 mM $NaHCO_3$ (Merck), 10 mM HEPES

Table 1 Sources of human material

Tissue	Healthy	Diseased
Liver	Partial hepatectomy, organ donation	Liver transplantation (recipient with ESLD)
Kidney	Tumor nephrectomy	ESRD nephrectomy, transplantectomy
Jejunum	Pancreaticoduodenectomy	NA
Ileum	Right hemicolectomy	Right hemicolectomy (patients with Crohn's disease)
Colon	Right hemicolectomy	NA
Lung	NA	Idiopathic pulmonary fibrosis

ESLD end-stage liver disease, *ESRD* end-stage renal disease, *NA* not available

(MP Biomedicals, Aurora, OH, USA), saturated with carbogen (95% O_2/5% CO_2), pH 7.42. Slices were incubated in Williams' medium E (WME, with L-glutamine, ThermoFisher Scientific, Landsmeer, The Netherlands) or Dulbecco's modified Eagle medium (DMEM, with L-glutamine, ThermoFisher Scientific) with different supplements. Table 2 summarizes the details of the preparation and incubation of murine and human PCTS.

Liver, kidney and lung PCTS had a wet weight of 4–5 mg and thickness of 200–250 µm, whereas intestinal slices had a wet weight of 1–2 mg and thickness of 300–400 µm. The preparation of human intestinal slices differed from mouse: after the luminal surface of human gut was flushed with ice-cold oxygenated KHB, the submucosa, muscular layer and serosa were gently removed from the intestinal mucosa.

All PCTS were cultured for 48 h at 37 °C in an 80% O_2/5% CO_2 atmosphere while shaken at 90 rpm. No pre-incubation step was used for culturing PCTS. Medium was refreshed after 24 h.

Sample collection

PCTS were collected immediately after slicing (0 h) and after 48 h incubation. For each animal/donor and time point, we used three slices for the viability assay, and four slices for NGS analysis. Samples were snap-frozen and stored at

Table 2 Preparation and incubation of human and murine PCTS

Tissue	Agarose	Preservation solution	Culture medium supplements	Final conc	Plating
Liver	–	UW	WME GlutaMAX™	–	Mouse and human: 12-well plate; 1.3 mL per well
			D-Glucose	25 mM	
			Gentamycin	50 µg/ml	
Kidney	–	UW	WME GlutaMAX™	–	Mouse and human: 12-well plate; 1.3 mL per well
			D-Glucose	25 mM	
			Ciprofloxacin	10 µg/mL	
Gut (jejunum, ileum and colon)	3% agarose in 0.9% NaCl	KHB	WME GlutaMAX™	–	Mouse: 24-well plate; 0.5 mL per well Human: 12-well plate; 1.3 mL per well
			D-Glucose	25 mM	
			Gentamycin	50 µg/ml	
			Fungizone	2.5 µg/ml	
Lung	1.5% agarose in 0.9% NaCl	UW	DMEM GlutaMAX™	–	Mouse and human: 12-well plate; 1.3 mL per well
			D-Glucose	25 mM	
			Non-essential amino acid mixture	0.1 mM	
			FCS	10%	
			Penicillin	100 U/mL	
			Streptomycin	100 µg/ml	
			Gentamycin	50 µg/ml	

Suppliers: WME GlutaMAX™ and DMEM GlutaMAX™ were purchased from ThermoFisher Scientific (Landsmeer, The Netherlands), D-glucose from Merck (Darmstadt, Germany), gentamycin and fungizone from Invitrogen (Paisley, Scotland), ciprofloxacin from Sigma-Aldrich (Saint Louis, USA), non-essential amino acid mixture, penicillin and streptomycin from Life Technologies (Bleiswijk, The Netherlands), fetal calf serum from Biowest (Nuaillé, France)

UW University of Wisconsin preservation solution, *KHB* Krebs–Henseleit buffer, *WME* Williams' medium E, *DMEM* Dulbecco's modified Eagle medium, *FCS* fetal calf serum

− 80 °C until further use. Additionally, culture medium from the wells with human slices used for NGS was collected at 24 h and 48 h, then stored at − 80 °C.

Viability

Viability of the tissue slices was measured with adenosine triphosphate (ATP) bioluminescence kit (Roche Diagnostics, Mannheim, Germany), as previously described (de Graaf et al. 2010). The ATP (pmol) was normalized to the total protein content (µg) estimated by the Lowry assay (Bio-Rad DC Protein Assay, Bio Rad, Veenendaal, The Netherlands).

RNA isolation and next-generation sequencing (NGS)

Total ribo-depleted RNA was extracted from PCTS semi-automatically with MagMax AM1830 kit (Fisher Scientific GmbH, Schwerte, Germany). Reverse transcription was performed with 100 ng RNA using TruSeq Stranded Total RNA LT Sample Prep Kit with Ribo-Zero™ H/M/R (Order #RS-122-2502, Illumina Inc, San Diego, CA, USA). The kit covers the transcription of protein-coding, non-coding and non-polyadenylated RNAs, while depleting cytoplasmic ribosomal RNA. The sequencing libraries were constructed according to the recommended procedures. Sequencing was carried out using the Illumina TruSeq methods (cluster kit TruSeq SR Cluster Kit v3-cBot-HS GD-401-3001, sequencing kit TruSeq SBS Kit HS- v3 50-cycle FC-401-3002) as 85 bp, single reads and 7 bases index read at depth of 50–60 million reads per sample on an Illumina HiSeq 3000 system.

Of note, the available lung PCTS (from five healthy mice and one patient with idiopathic pulmonary fibrosis) were sequenced together with other samples, but were excluded from the downstream analyses due to the lack of human healthy lung samples and insufficient number of biological replicates for human diseased lung PCTS.

NGS bioinformatics analysis

The processing pipeline was previously described (Söllner et al. 2017). RNA-Seq reads from all samples were aligned to the human and mouse reference genomes, respectively (Ensembl 70; http://www.ensembl.org) using STAR. Gene expression levels were quantified using Cufflinks software (Trapnell et al. 2013) to obtain the reads per kilobase of transcript per million mapped reads (RPKM), as well as read counts. The matrix of read counts and the design files were imported to R, normalization factors were calculated using trimmed mean of *M* values and subsequently normalized before further downstream analysis.

Differentially expressed genes (DEGs) were identified for all experimental groups. Paired differential gene expression (e.g. PCTS 48 h vs. 0 h) was assessed by Limma with a paired design for multiple samples originated from the same animal/donor. Fold changes (FC) were $\log_2$ normalized and *p* values were adjusted for false discovery rate (FDR) by applying Benjamini–Hochberg correction. Genes with a p_{adj} value ≤ 0.01 and $\log_2$ (FC) ≥ 1 were considered as differentially expressed. Graphs illustrating top 10 regulated DEGs were created using D3.js JavaScript library (http://d3js.org/).

Principal component analysis and hierarchical clustering

Principal component analysis (PCA) was performed on limma voom-transformed log (counts per million) using R. We used the first three principal components (PCs) to produce two-dimensional plots with Python scientific library Matplotlib. The heatmap of $\log_2$ (FC) gene expression of murine and human PCTS was generated with the online tool Morpheus (https://software.broadinstitute.org/morpheus/).

Pathway analysis

Functional pathway analysis of differentially expressed gene sets was performed with QIAGEN Ingenuity® Pathway Analysis software (IPA®, QIAGEN Redwood City, CA, USA) for the following sets of genes: (1) culture-induced DEGs in murine and human tissue slices; (2) DEGs between diseased and healthy control human PCTS that were concurrently present at 0 h or 48 h; (3) common DEGs in cultured healthy and diseased human PCTS. These sets of DEGs with corresponding gene identifiers (Ensembl gene ID), $\log_2$ (FC) values and adjusted *p* values were uploaded into the IPA to reveal the enriched canonical signalling pathways according to the Ingenuity Pathways Knowledge Base (IPKB). To assess whether a biological pathway significantly underlies the data, we used two independent scores: a *p* value (i.e. Fisher's exact test *p* value) that measures significance of overlap between observed and predicted sets of regulated genes, and a *z*-score that measures the match of observed and predicted up-/downregulation patterns (Krämer et al. 2014). The sign of *z*-score determines whether the pathway is predicted to be activated or inhibited. In cases of insufficient literature-based evidence, the *z*-score is undetermined. Canonical pathways with *p* value ≤ 0.01 and $|z\text{-score}| \geq 2$ were considered significantly regulated (Krämer et al. 2014).

Cytokine release

Culture supernatants, collected after 24 h and 48 h, were used for quantification of chemokine and cytokine levels by Meso Scale Discovery (MSD) multiplex assay. The mesoscale platform (Meso Scale Discovery, Gaithersburg, Md., USA) employs electroluminescence technology allowing for simultaneous measurement up to ten analytes with

high sensitivity. Samples were measured with MSD SECTOR S600 Reader using MSD DISCOVERY Workbench Software according to the manufacturer's instructions. The list of selected analytes with corresponding catalogue numbers is provided in Table S2. Measurement of 24-h and 48-h medium samples was carried out separately; absolute concentrations (pg/mL) were normalized to the negative control (i.e. medium that was neither in contact with PCTS nor under influence of incubator conditions). For each cytokine, we used the sum of 24-h and 48-h measurements to determine the total cytokine concentration. Only those cytokines that had a total concentration higher than 20 pg/mL in at least one experimental group and were regulated on gene level [with a p_{adj} value ≤ 0.01 and $\log_2$ (FC) ≥ 1] during culture were included for further analysis. Data are presented as heatmap of normalized absolute concentrations of secreted cytokines, with applied average-linkage clustering (performed using Pearson correlation). The heatmap was generated using the online tool Morpheus (https://software.broadinstitute.org/morpheus/). The correlation between cytokine release (as measured by MSD) and gene expression was made by comparing total cytokine concentrations to the average gene expression (RPKM values) of PCTS at 0 h and 48 h (geometric mean from each timepoint). We applied a simple linear regression model (TIBCO Spotfire Analyse 7.11.0) and resulting r^2 coefficient was used to assess the strength of the correlation.

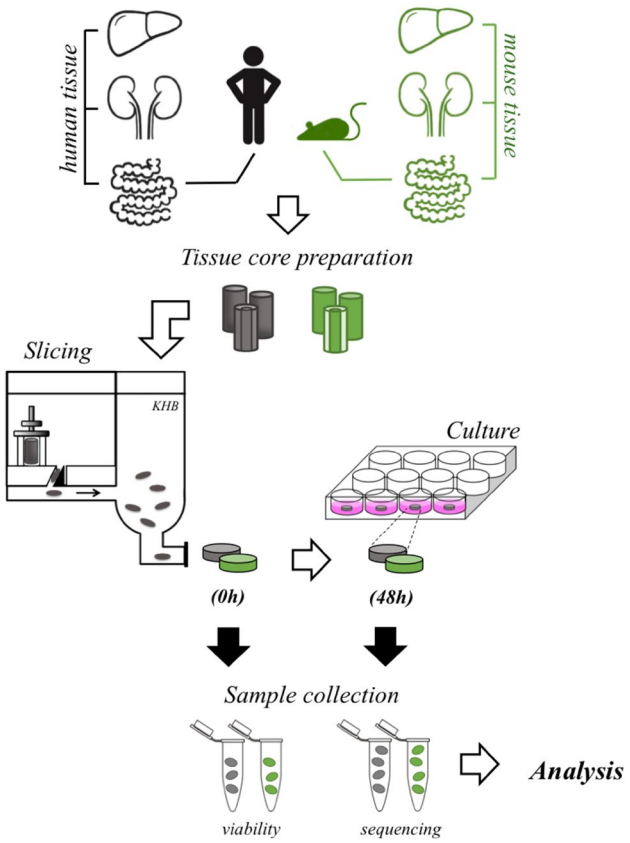

Fig. 1 Study workflow. Precision-cut tissue slices (PCTS) were prepared from murine or human tissues (liver, kidney, jejunum, ileum and colon) using Krumdieck tissue slicer and incubated for 48 h. Samples were collected at 0 h (prior incubation) and at 48 h for viability measurement and sequencing analysis

Part I: Next-generation sequencing reveals in-depth features of healthy murine and human precision-cut tissue slices

Results of Part I

Part I of this study was undertaken to characterize the transcriptional profiles of murine and human PCTS as well as their change over time in culture. Only healthy tissues were used to prepare murine and human PCTS for Part I study. Figure 1 depicts the Part I workflow. We cultured murine and human PCTS for 48 h as previous studies reported that at 48 h slices largely retain tissue viability and structural integrity (Stribos et al. 2016; Luangmonkong et al. 2017; Bigaeva et al. 2019). Lung PCTS were prepared and cultured as described in "Methods", but hereafter excluded from functional analyses (and, therefore, omitted in Fig. 1) because we were only able to collect lung slices from healthy mice, but not from healthy human donors due to the extremely limited availability of resected human lung tissue. Figure S1a, b shows that all PCTS remained viable during the 48 h of culture. We observed high variability for the RNA quality across the organs, with intestine PCTS having generally the lowest RNA quality based on RNA integrity numbers (data not shown). Nevertheless, since the total RNA protocol allows for sequencing samples with partially degraded RNA, we could include all samples into the analysis. After sequencing, we obtained for each sample 25–75 million single end reads with a rate of 40–60% unique mapping to exonic regions of non-ribosomal protein-coding genes (data not shown). Consequently, the sequencing data were sufficient to investigate differential expression between all groups of interest.

As a preliminary experiment, we investigated the sequencing variability of mouse liver PCTS obtained from one animal. We observed a very low intra-individual variability in murine PCTS; therefore, we only included one single mouse organ slice per animal per condition into the analysis. In case of human PCTS, we included 3–4 slices per donor per condition (technical replicates) since the variability was generally higher in human samples compared to mouse. However, these replicates showed a very high reproducibility and low intra-individual variability, similar to the animal PCTS.

(Ia) Principal component analysis and hierarchical clustering

As a first step of the Part I study, we analysed murine and human PCTS data by principal component analysis (PCA) to investigate which experimental factors (organ, time in culture) have the strongest effect on the variance of the data. Two-dimensional plots based on first three components (PC1, PC2 and PC3) are shown in Fig. 2a–d. First two dimensions (PC1 vs. PC2) clearly separated murine PCTS samples by the tissue type (Fig. 2a). Mouse liver PCTS formed a distinct cluster along PC1 (bottom left). A second cluster is composed of the kidney samples (top left). All samples from intestinal PCTS (i.e. jejunum, ileum and colon) clustered together at the right part of the plot. In PC1 vs. PC3 (Fig. 2b), we observed clustering of the mouse samples based on culture time: 0-h PCTS (bottom of the plot) were separated from 48-h PCTS (top of the plot). Similar to murine PCTS, PC1 of human PCTS showed a consistent separation by tissue type with the liver samples clustering on the left with negative PC1 values, GI tract samples on the right with positive PC1 values and the kidney samples in between (Fig. 2c, d). PC3 showed an additional separation between human liver and kidney PCTS, whereas PC2 separated them by time in culture. Percentages of explained variance for each of the first three principal components are indicated in Fig. S2, which illustrates PCA results for all analysed PCTS (healthy murine PCTS in Fig. S2a, b; healthy and diseased human PCTS in Fig. S2c, d), including murine and human lung slices. Overall, PCA showed consistently that both murine and human PCTS can be distinguished by the tissue type and incubation time point, indicating that these two factors are the main drivers of variance involved in PCTS culture. Hierarchical clustering of differentially expressed genes with time in culture [$\log_2$ (FC); see Fig. 2e] showed that murine intestinal PCTS clustered first together and then with human intestinal PCTS. Along with species-specific clusters of differentially expressed genes (DEGs) (which might also originate from batch effects from comparing the results of two sequencing experiments, i.e. murine and human PCTS), there were organ-specific clusters of DEGs in murine and human PCTS, which have been investigated in more detail in the next section.

(Ib) Culture-induced changes in transcriptional profiles of murine and human PCTS

Total number of differentially expressed genes

To determine the global changes in the transcriptional profiles of PCTS during culture, we identified genes differentially expressed prior (0 h) and after culture (48 h) in murine and human PCTS from the five studied organs. We selected DEGs based on $\log_2$ (FC) ≥ 1 and p_{adj} value ≤ 0.01. Figure 3a, b illustrates the total numbers of identified DEGs (upregulated and downregulated) in murine and human PCTS from various organs. Figure S1c, d shows volcano plots that summarize FC and significance for all genes in each comparison. Lists of all DEGs in murine and human PCTS are provided in File S1. Generally, the observed transcriptional changes in PCTS during culture were strong because the number of DEGs was in the order of thousands. Interestingly, human jejunum PCTS had the lowest number of DEGs (563) compared to other human organs. The ratio between upregulated and downregulated DEGs was approximately 1:1 for all PCTS, except for mouse colon and human kidney, where the number of downregulated DEGs reached $\geq 60\%$. These results confirm that PCTS culture induced substantial changes in gene expression in both mouse and human tissues.

For a more detailed analysis of the transcriptional changes in each organ, we cross-referenced the DEGs in murine and human PCTS (with 1:1 homology) to identify which genes commonly expressed in both species are changed in the same or opposite direction. Figure 3c illustrates the pairwise comparisons of murine and human PCTS per organ. Although murine and human PCTS shared genes changed in the same direction during culture, the majority of DEGs ($> 55\%$) were regulated antagonistically or solely in one species. On the other hand, 10–40% of downregulated or upregulated DEGs were shared in expression and direction of change between murine and human PCTS. Due to the fact that the total numbers of DEGs in human PCTS were generally lower than in murine PCTS, the ratio of common vs. different DEGs was higher in human PCTS. As an example, the common genes (125 DEGs) between mouse and human jejunum PCTS represented 42% of total human DEGs and only 6% of mouse DEGs (Fig. 3c). Taken together, we showed that murine and human PCTS shared sets of similarly regulated genes during culture; however, most of the genes were not regulated in the same direction (File S2).

Top ten regulated genes in murine and human PCTS during culture

To further investigate transcriptional changes in PCTS, we aimed to determine the most differentially regulated genes in every mouse and human organ. Figure 4 illustrates the top ten upregulated genes and top ten downregulated genes with the most pronounced change in expression after 48 h [p_{adj} value ≤ 0.01 and $\log_2$ (FC) ≥ 1]. The top ten genes were ranked based on the absolute $\log_2$ (FC) values. Additional information regarding ensemble gene ID, target class and function of proteins encoded by the top ten genes is provided in Table S3 (mouse) and Table S4 (human). Complete DEGs

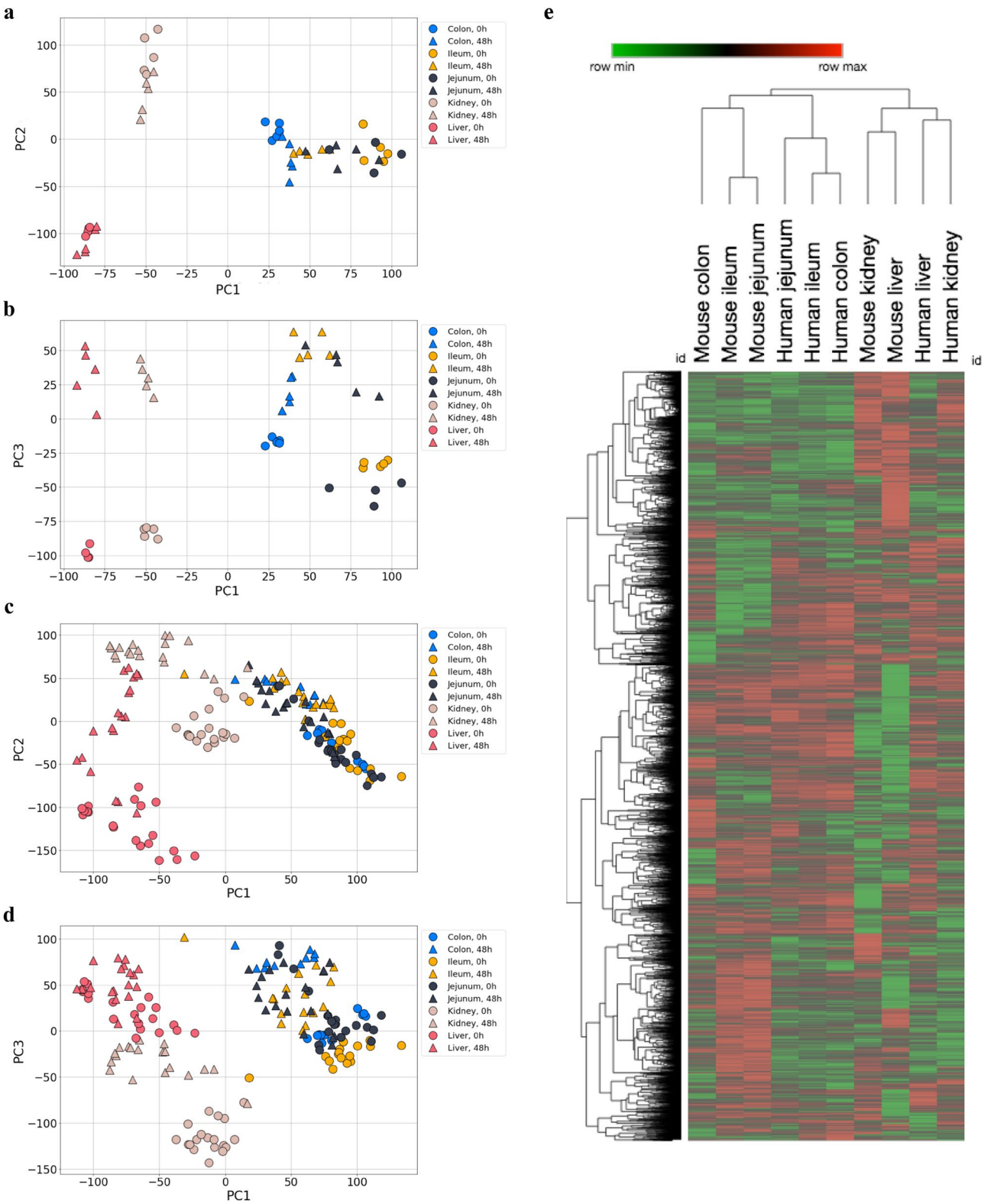

Fig. 2 Principal component analyses (PCA) and hierarchical clustering analysis in murine and human PCTS. PCA scatter plots of dimensions PC1 vs. PC2 and PC1 vs. PC3 in mouse PCTS (**a** and **b**) and human PCTS (**c** and **d**); $n = 5$. Samples are coloured by tissue type and shaped by incubation time point. Each symbol in the plots for murine and human PCTS represents total mRNA sequencing from a single technical replicate. **e** Transcriptomic profiles of murine and human PCTS during culture. The heatmap of $\log_2$ (FC) values illustrates expression of 8360 genes (with $p_{adj} \leq 0.01$) regulated during 48-h culture in murine and human PCTS (1:1 homology). Average-linkage hierarchical clustering was performed using Pearson correlation

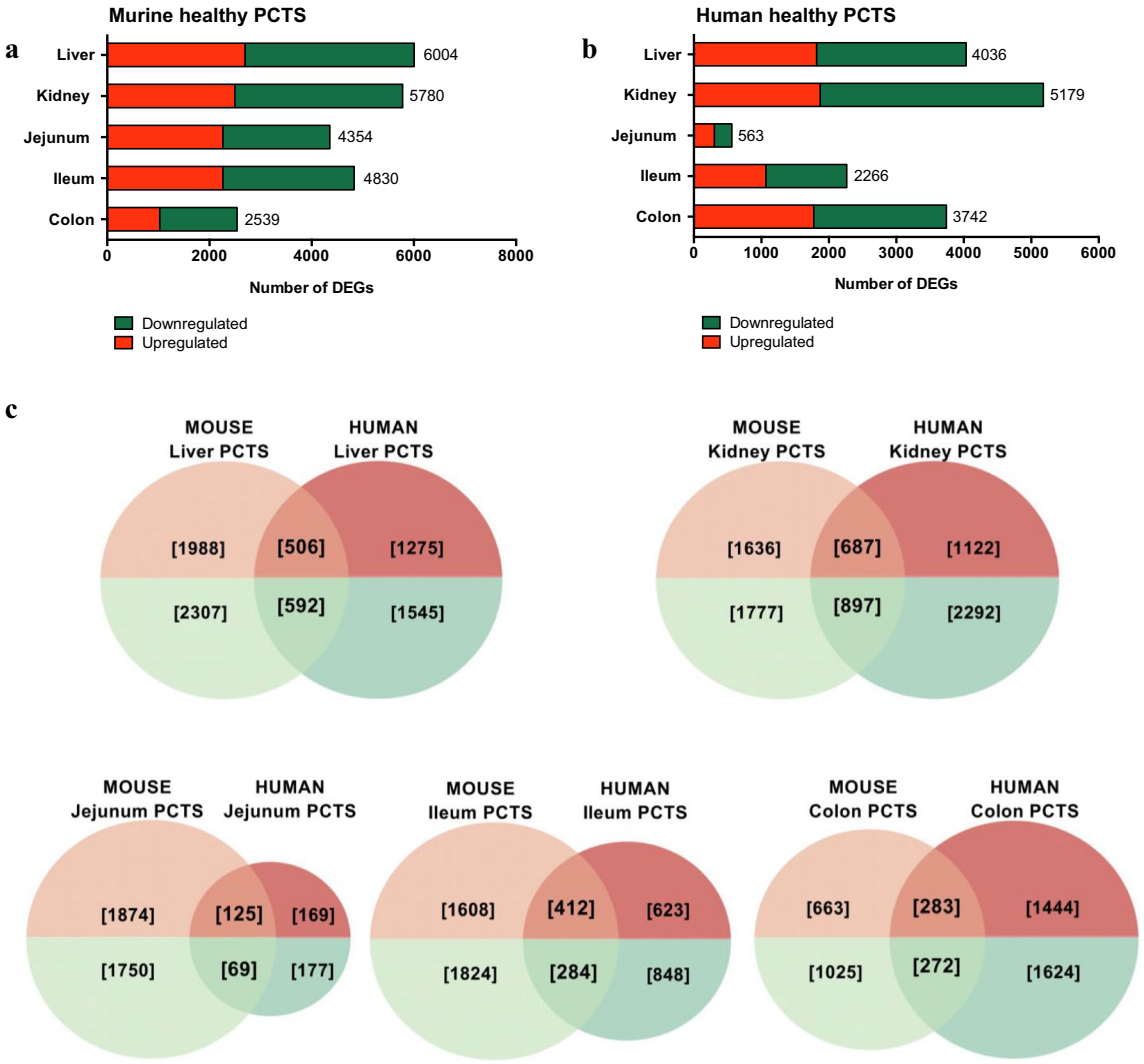

Fig. 3 Differentially expressed genes in murine and human PCTS during culture. DEGs were defined as genes with $\log_2$ (FC) ≥ 1 and p_{adj} value ≤ 0.01. **a** Total number of DEGs, upregulated and downregulated, in mouse PCTS. **b** Total number of DEGs, upregulated and downregulated, in human PCTS. Full lists of identified DEGs are provided in File S1. **c** Venn diagrams showing the number of unique genes regulated in mouse and human PCTS and the number of overlapping genes. Red colour indicates upregulated set of DEGs, green colour indicates the downregulated (colour figure online)

lists can be found in File S1. Further observations are based solely on the lists of the top ten regulated genes.

Murine PCTS The most upregulated genes in murine PCTS during culture were mainly related to inflammation (*Il11, Il6, Cxcl1, Cxcl2, Cxcl5, Cxcl5, Ccl2, Ccl7, Ccl20* and *Gpnmb*) and extracellular matrix (ECM) organization (*Mmp3, Mmp10, Mmp13, Timp1*). Inflammatory gene *Il11* was commonly upregulated in mouse kidney, ileum and colon; *Il6* was common for kidney and ileum. *Mmp3* was highly upregulated in all mouse intestinal PCTS; jejunum and colon additionally highly expressed *Mmp10*. Mouse kidney showed highly upregulated *Havcr1*, encoding kidney injury molecule-1 (KIM-1), a marker of acute renal tubular injury. Moreover, genes encoding enzymes were often present in top ten upregulated DEGs (*Sult1e1, Has2, Tat, Sis)* in various organs.

The most downregulated genes can be grouped in two main categories: metabolic enzymes (*Cyp2d12, Cyp7a1, Sult2a8, Elovl3*, etc.) and transporters (*Slc5a4a, Slc5a11, Slc5a12, Slc13a2OS, Slc13a2, Slc22A28, Slc22a30, Slc28a1, Slc34a1, Slc34a3, Slco1a4*). Mouse liver PCTS showed the highest number of genes encoding enzymes. Most genes encoding transporters were found in top ten downregulated genes in mouse jejunum, whereas no such genes were present in mouse colon. However, genes encoding transporters were also present in top ten upregulated genes, as shown by *Slc7a11* in mouse liver and kidney PCTS.

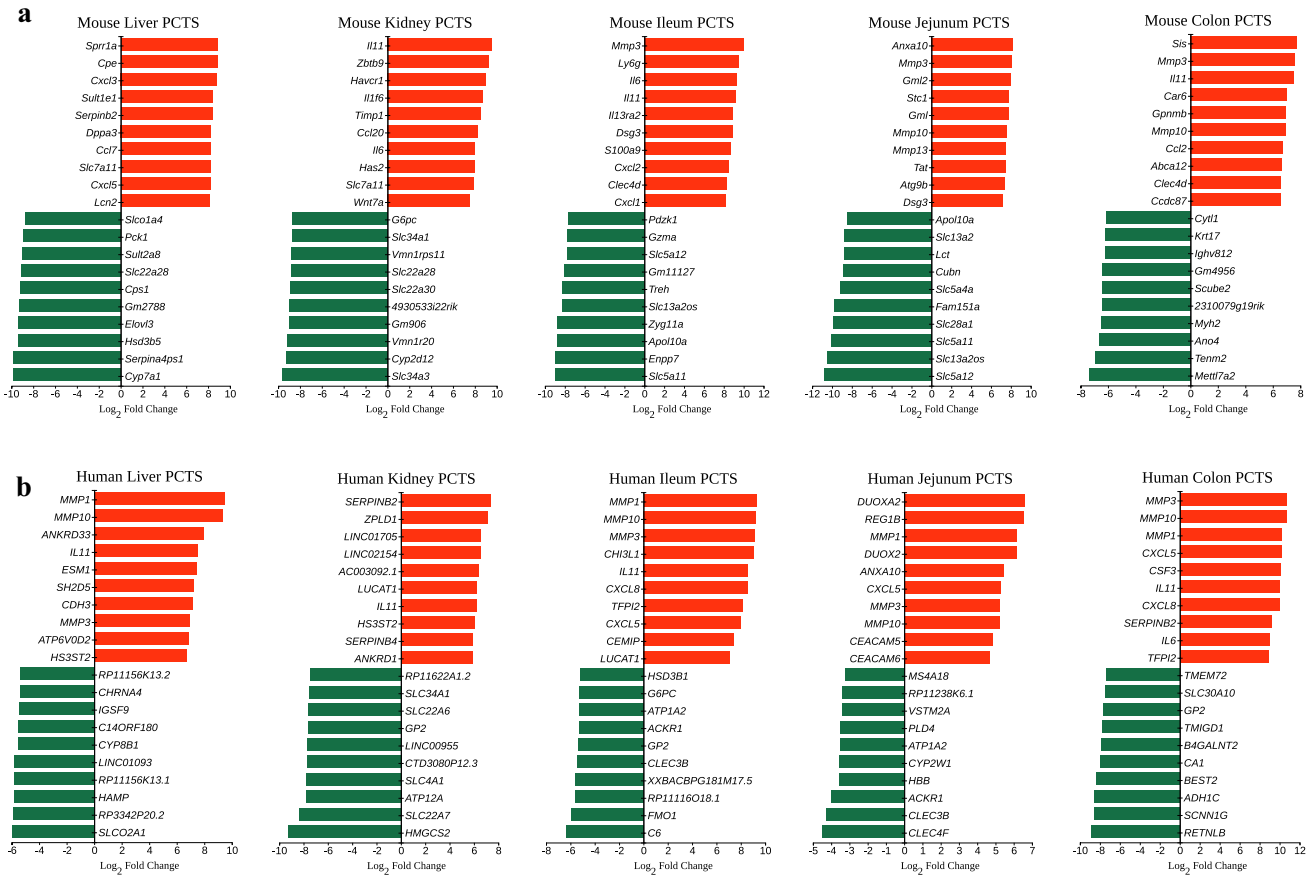

Fig. 4 Top ten significantly upregulated and downregulated DEGs in murine and human PCTS. Genes were selected based on the $\log_2$ (FC) values. **a** Mouse PCTS; **b** human PCTS. Full lists of DEGs are provided in File S1, and the detailed description of top ten genes is provided in Table S3 (mouse) and Table S4 (human)

Human PCTS Similar to murine PCTS, the top ten upregulated genes in human PCTS belonged mostly to inflammation (*IL11, IL6, CXCL5, CXCL8, CSF3*), ECM organization (*MMP1, MMP3, MMP10, TFPI2*) and catalysts (*DUOXA2, ATP6V0D2, HS3ST2, CEMIP)*. Human ileum and colon showed upregulation for most of these genes, while jejunum and liver had less inflammation-related genes and human kidney had no ECM-related genes. *MMP1, MMP3* and *MMP10* were found in all human PCTS, except kidney. *IL11* was common in human kidney, ileum and colon; *CXCL5* was shared by all intestinal PCTS, while ileum and colon additionally highly expressed *CXCL8*. Human jejunum PCTS showed highly upregulated enzyme-coding gene *DUOX2* and associated gene *DUOXA2*; *HS3ST2* was found in top ten upregulated genes in human liver and kidney. Moreover, top ten upregulated genes in human kidney included several non-protein-coding transcripts.

Similar to murine PCTS, top ten downregulated genes in human PCTS included genes encoding enzymes (*CYP8B1, CYP2W1, ATP1A2, HMGCS2, PLD4, HSD3B1, G6PC, FMO1, CA1* and *ADH1C*) and transporters (*SLCO2A1, SLC4A1, SLC22A6, SLC22A7, SLC30A10, SLC34A1, BEST2, SCNN1G*). Gene *GP2* was commonly downregulated in human kidney, ileum and colon. Of note, ten novel transcripts were identified among the top downregulated genes in human liver, kidney, jejunum and ileum.

Commonly regulated top genes in murine and human PCTS Genes that were common across most of the mouse and human organs included *IL11, MMP3* and *MMP10* (Fig. 4). Moreover, *CXCL5* was highly expressed by human intestinal PCTS and mouse liver. In turn, *SERPINHB2*, encoding PAI-2, was upregulated in mouse liver, human kidney and human colon PCTS. Same organs, but from different species (mouse and human), shared expression of several transcripts: for example, mouse and human kidney PCTS had common upregulation of *IL11* and downregulation *of SLC34A1*; mouse and human jejunum shared high expression of *ANXA10* and *MMP10*; mouse and human ileum—*IL11* and *MMP3*; mouse and human colon—*IL11*, *MMP3* and *MMP10*.

Enriched biological pathways in murine and human PCTS in culture

Next, we determined the biological processes associated with the culture-induced changes reflected by the DEGs. For this purpose, we performed functional enrichment analysis using IPA to identify canonical pathways altered in murine and human PCTS during culture. The ranking of canonical pathways was based on the *z*-score: a *z*-score ≥ 2 (predictor of activation) or ≤ -2 (predictor of inhibition) was considered as meaningful (Krämer et al. 2014). Pathways with a *p* value ≥ 0.01 and unidentified *z*-score were omitted from the analysis. Figures 5 and 6a show the top five canonical pathways activated or inhibited during culture in murine PCTS and human PCTS, respectively. To make a thorough examination, further observations are based on complete lists of significantly altered canonical pathways in PCTS that are provided in Figs. S3–9. We found that six canonical pathways activated during culture were present in most mouse organs and, interestingly, they were similar to the pathways prevalent in human PCTS. These included IL-6 signalling, IL-8 signalling, HMGB1 signalling, osteoarthritis pathway,

		Canonical Pathway	z-score	-log(p-value)	Size	Downregulated (%)	Upregulated (%)	Overlap (%)
Activated pathways	Liver	iNOS Signaling	3,64	2,95	45	20	69	89
		PI3K/AKT Signaling	3,57	2,23	131	28	59	87
		LPS/IL-1 Mediated Inhibition of RXR Function	3,39	19,70	222	55	27	82
		HMGB1 Signaling	3,32	2,18	139	30	55	85
		Agrin Interactions at Neuromuscular Junction	3,14	3,17	75	37	56	93
	Kidney	Ephrin Receptor Signaling (*)	4,26	8,64	179	23	66	89
		IL-6 Signaling	4,18	7,67	134	20	66	87
		HMGB1 Signaling	4,11	7,88	139	24	60	85
		Actin Nucleation by ARP-WASP Complex (*)	3,90	6,30	62	15	74	89
		Acute Phase Response Signaling (*)	3,87	5,56	176	29	57	86
	Jejunum	Osteoarthritis Pathway (*)	3,91	10,00	212	25	57	82
		Cholecystokinin/Gastrin-mediated Signaling	3,78	2,18	107	27	61	88
		IL-8 Signaling (*)	3,68	3,30	203	31	58	89
		STAT3 Pathway	3,31	4,18	103	32	64	97
		IL-6 Signaling (*)	3,18	2,04	134	26	60	87
	Ileum	IL-6 Signaling	4,22	3,12	134	28	58	87
		Acute Phase Response Signaling	4,00	3,54	176	37	48	86
		Toll-like Receptor Signaling	3,90	2,30	76	30	57	88
		STAT3 Pathway	3,67	4,70	103	36	61	97
		NF-κB Signaling	3,27	3,98	187	33	51	84
	Colon	HMGB1 Signaling (*)	2,65	4,31	139	31	52	85
		IL-8 Signaling (*)	2,53	5,06	203	34	54	89
		ILK Signaling	2,47	8,01	197	35	48	84
		NRF2-mediated Oxidative Stress Response	2,36	3,49	199	34	50	86
		Ceramide Signaling	2,36	2,23	99	38	54	93
Inhibited pathways	Liver	Oxidative Phosphorylation	-7,35	8,98	109	77	6	83
		LXR/RXR Activation (*)	-5,61	15,30	121	53	31	83
		Nicotine Degradation II (*)	-5,58	7,21	65	68	6	74
		Nicotine Degradation III	-5,01	5,62	56	66	7	73
		Superpathway of Cholesterol Biosynthesis	-4,90	11,50	28	89	7	96
	Kidney	Oxidative Phosphorylation	-7,00	7,61	109	81	2	83
		PPAR Signaling	-5,10	3,92	101	20	63	83
		PPARα/RXRα Activation	-4,81	5,30	186	33	50	83
		LXR/RXR Activation (*)	-4,64	5,13	121	34	50	83
		TCA Cycle II (Eukaryotic)	-3,87	4,85	24	92	4	96
	Jejunum	PPAR Signaling (*)	-4,16	2,56	101	25	58	83
		LXR/RXR Activation	-4,04	2,78	121	32	50	83
		Inhibition of Matrix Metalloproteases	-2,98	7,04	39	15	72	87
		PTEN Signaling	-2,96	2,53	125	39	50	91
		Fatty Acid β-oxidation I	-2,84	4,26	32	72	25	97
	Ileum	PPAR Signaling (*)	-4,24	3,36	101	29	53	83
		LXR/RXR Activation (*)	-4,12	3,44	121	42	40	83
		PPARα/RXRα Activation	-3,20	3,47	186	39	44	83
		Calcium-induced T Lymphocyte Apoptosis	-3,13	3,64	66	50	26	76
		iCOS-iCOSL Signaling in T Helper Cells	-2,79	3,62	123	43	36	80
	Colon	Calcium Signaling	-3,89	6,50	206	48	27	77
		Synaptic Long Term Depression	-3,89	4,39	180	48	34	83
		Neuropathic Pain Signaling In Dorsal Horn Neurons	-3,84	2,89	115	58	30	85
		GPCR-Mediated Nutrient Sensing in Enteroendocrine Cells	-2,84	2,67	112	51	33	87
		CREB Signaling in Neurons	-2,75	3,65	218	47	36	85

Fig. 5 Top five canonical pathways that were significantly changed during culture in murine PCTS as identified by ingenuity pathway analysis (IPA). Only pathways with *p* value ≤ 0.01 and a *z*-score ≥ 2 (predictor of activation) or ≤ -2 (predictor of inhibition) were included. Pathway size (i.e. total number of genes in a pathway), percentage of significantly downregulated (green bars) and upregulated (red bars) genes in a given pathway, and percentage of overlap with the dataset (grey bars) are indicated for each pathway. Pathways in blue colour are most common across the organs. Pathways marked with (asterisk) are shared between mouse and human respective organ. Full lists of significantly changed pathways in murine PCTS from each organ are provided in Fig. S3–5 (colour figure online)

a

		Canonical Pathway	z-score	-log(p-value)	Size	Downregulated (%)	Upregulated (%)	Overlap (%)
Activated pathways	Liver	Integrin Signaling	4,26	6,23	219	23	51	75
		IL-8 Signaling	3,78	6,26	203	26	52	78
		Signaling by Rho Family GTPases	3,68	4,26	252	28	50	79
		Rac Signaling	3,66	2,16	123	23	50	75
		Actin Nucleation by ARP-WASP Complex	3,44	4,43	62	18	58	76
	Kidney	PI3K/AKT Signaling	4,49	2,14	131	23	53	76
		Actin Nucleation by ARP-WASP Complex (*)	4,08	4,34	62	18	58	76
		Ephrin Receptor Signaling (*)	3,18	2,60	179	32	47	80
		Acute Phase Response Signaling (*)	3,00	3,56	176	32	50	82
		Remodeling of Epithelial Adherens Junctions	2,83	2,32	69	17	57	74
	Jejunum	Acute Phase Response Signaling	3,32	2,70	176	38	45	82
		Osteoarthritis Pathway (*)	3,00	5,87	212	29	51	80
		IL-6 Signaling (*)	3,00	2,51	134	28	48	76
		Superpathway of Cholesterol Biosynthesis	2,71	11,10	28	18	64	89
		IL-8 Signaling (*)	2,71	2,23	203	33	43	78
	Ileum	Osteoarthritis Pathway	3,67	6,51	212	28	52	80
		Role of IL-17F in Allergic Inflammatory Airway Diseases	3,61	5,04	46	15	54	70
		TREM1 Signaling	3,44	5,29	75	24	60	84
		IL-8 Signaling	3,31	4,49	203	25	52	78
		Dermatan Sulfate Biosynthesis	3,05	3,17	59	31	49	80
	Colon	IL-8 Signaling (*)	4,73	3,51	203	25	53	78
		HMGB1 Signaling (*)	4,52	7,95	139	21	55	76
		PI3K/AKT Signaling	4,38	3,21	131	18	57	76
		Acute Phase Response Signaling	4,22	5,14	176	22	61	82
		TREM1 Signaling	4,15	3,09	75	20	63	84
Inhibited pathways	Liver	LXR/RXR Activation (*)	-5,17	25,90	121	62	32	94
		Nicotine Degradation II (*)	-3,96	5,15	65	57	18	75
		Estrogen Biosynthesis	-3,90	6,43	41	61	22	85
		Fatty Acid β-oxidation I	-3,77	7,80	32	69	22	94
		Melatonin Degradation I	-3,71	4,09	65	58	20	78
	Kidney	Neuropathic Pain Signaling In Dorsal Horn Neurons	-3,77	2,25	115	50	31	83
		LXR/RXR Activation (*)	-3,21	4,80	121	55	40	94
		Fatty Acid β-oxidation I	-3,21	3,40	32	81	13	94
		Serotonin Degradation	-3,16	4,84	77	61	16	77
		Ethanol Degradation II	-2,98	5,69	37	68	14	81
	Jejunum	PPAR Signaling (*)	-2,65	2,13	101	20	54	74
	Ileum	LXR/RXR Activation (*)	-3,44	4,07	121	33	61	94
		PPAR Signaling (*)	-3,44	3,41	101	18	56	74
		Nicotine Degradation II	-2,89	2,29	65	58	15	75
		Estrogen Biosynthesis	-2,33	2,35	41	63	20	85
		Superpathway of Melatonin Degradation	-2,31	2,03	70	63	16	80
	Colon	Oxidative Phosphorylation	-6,86	13,40	109	72	4	75
		PPAR Signaling	-5,24	7,16	101	16	58	74
		PPARα/RXRα Activation	-3,55	4,47	186	28	44	73
		LXR/RXR Activation	-3,53	3,51	121	35	59	94
		PTEN Signaling	-3,16	3,24	125	22	50	73

b

		Mouse PCTS	Human PCTS	Common pathways
Activated	Liver	17	34	5
	Kidney	62	14	10
	Jejunum	28	9	4
	Ileum	14	21	8
	Colon	9	59	6
Inhibited	Liver	58	26	18
	Kidney	29	16	8
	Jejunum	9	1	1
	Ileum	11	6	2
	Colon	10	9	0

Fig. 6 Top five canonical pathways that were significantly changed during culture in human PCTS as identified by ingenuity pathway analysis (IPA). Only pathways with p value ≤ 0.01 and a z-score ≥ 2 (predictor of activation) or ≤ -2 (predictor of inhibition) were included. Pathway size (i.e. total number of genes in a pathway), percentage of significantly downregulated (green bars) and upregulated (red bars) genes in a given pathway, and percentage of overlap with the dataset (grey bars) are indicated for each pathway. **a** Pathways in blue colour are most common across the organs. Pathways marked with (asterisk) are shared between mouse and human respective organ. Complete lists of significantly changed pathways in human PCTS from each organ are provided in Figs. S6–9. **b** Based on the complete lists, we determined the total numbers of altered canonical pathways in murine and human PCTS, as well as the number of shared pathways in each organ (colour figure online)

acute phase response signalling and LPS/IL-1-mediated inhibition of RXR function. Among the prevalent canonical pathways that showed inhibition during culture for both mouse and human organs were LXR/RXR activation, PPAR signalling and fatty acid β-oxidation I. Furthermore, three additional pathways—ceramide signalling, STAT3 pathway and NF-κB signalling—were activated solely in mouse organs, while PPARα/RXRα activation pathway was inhibited. In turn, human PCTS additionally showed common activation of PI3K/AKT signalling and inhibition of valine degradation I. Figure 6b illustrates that all organ PCTS shared a number of pathways in both species, except for the inhibited pathways in colon. Overall, the enriched pathways associated with DEGs give a detailed insight into the biological processes that are driven by culture-induced transcriptional changes in PCTS.

(Ic) Regulation of selected canonical pathways in murine and human PCTS during culture

Since PCTS are used as a model for fibrosis and inflammation (Westra et al. 2013; Stribos et al. 2017), we focused on specific canonical pathways that are related to these pathophysiological processes, including fibrosis (and ECM organization), inflammation, apoptosis, hypoxia, etc. With this in mind, we used the aforementioned IPA to evaluate the changes in these pathways of interest (Fig. 7). For each pathway, we recorded the following information: significance (reflected by a p value ≤ 0.01) and the direction of change (reflected by the z-score, when available). Genes associated with each selected Ingenuity canonical pathway are provided in File S3.

Fibrosis-associated signalling pathways

All mouse organ PCTS showed significant changes during 48 h of culture. Liver and ileum had the lowest number of significantly changed fibrosis-associated canonical pathways (5 out of 18), while kidney had the most pathways changed (17 out of 18). Based on a z-score, culture typically activated fibrosis pathways; with the exception of PI3K/AKT pathway, which was inhibited in jejunum PCTS. Compared to other murine organs, kidney PCTS had the highest number of the activated pathways (10 out of 18). In contrast, IPA could not predict the direction of change for any selected pathway in colon PCTS, although seven pathways were significantly changed. TGF-β signalling, one of the main drivers of fibrosis (Meng et al. 2016), showed a significant change during culture of kidney, jejunum and colon PCTS; furthermore, this canonical pathway was activated in kidney and ileum.

Similar to murine PCTS, all human organs showed significant changes in the fibrosis-related pathways during culture (Fig. 7). The number of significantly changed canonical pathways (based on p value) varied, with jejunum PCTS having the lowest (1 out of 18) and liver and colon the highest (9 and 10 out of 18, respectively). The direction of change in the selected pathways was activation, with one exception—inhibition of FGF signalling in kidney PCTS. Most activated pathways were observed in colon PCTS (12 out 18), followed by liver PCTS with seven pathways. The other three organs only showed activation for p38 MAPK signalling (jejunum and ileum) and PI3K/AKT signalling (kidney and ileum).

ECM organization

We selected two pathways for ECM organization: inhibition of matrix metalloproteases and integrin signalling (Fig. 7). Murine PCTS showed that both canonical pathways were significantly changed during culture in all organs, except inhibition of matrix metalloproteases in liver and kidney PCTS. Regarding the direction of change, integrin signalling was activated only in kidney slices, whereas inhibition of matrix metalloproteases was changed in both directions: activated in jejunum PCTS (i.e. more inhibition of MMPs) and inhibited in kidney and colon PCTS (i.e. activation of MMPs).

As for human slices, significant inhibition of matrix metalloproteases (except kidney) and integrin signalling (except jejunum) were identified. Only integrin signalling showed a direction of change—activation in liver and colon PCTS.

Inflammation-related canonical pathways

Next, we analysed 22 canonical pathways associated with inflammation. After culture, all murine organ PCTS showed a significant change for at least one-third of these pathways (Fig. 7). The most significant differences were observed in kidney PCTS (17 out of 22 pathways). Five pathways were significantly changed in all organ PCTS: dendritic cell maturation, IL-6, IL-8, IL-10 signalling and LPS/IL-1-mediated inhibition of RXR function. Further, we observed that out of 22 inflammation-associated pathways, 13 displayed a direction of change. Inhibition was observed only for one pathway—chemokine signalling in jejunum PCTS. Kidney and liver slices had the most activated pathways (eight and six, respectively), while the other organs had a similar number of activated pathways (three and five).

Likewise, inflammation-associated pathways were altered during the culture of human PCTS. The total number of significantly changed pathways was smaller in human PCTS than in mouse. Most differences were observed for colon and ileum, where 14 and 11 pathways out of 22 were changed, respectively. The other three organs showed differences for only few pathways, with jejunum having the lowest number of significantly changed pathways (four). The evaluation

Fig. 7 Regulation of preselected pathways in murine and human PCTS during 48-h culture. Purple colour indicates a significant pathway change based on a p value ≤ 0.01; whereas predicted pathway activation (A) or inhibition (I) is indicated by a z-score, if available (colour figure online)

	Ingenuity Canonical Pathways	Mouse					Human				
		Liver	Kidney	Jejunum	Ileum	Colon	Liver	Kidney	Jejunum	Ileum	Colon
Fibrosis-associated signaling pathways	BMP signaling pathway		A								A
	EGF Signaling										
	ERK/MAPK Signaling										A
	FGF Signaling							I			A
	Hepatic Fibrosis / Hepatic Stellate Cell Activation										
	HGF Signaling										A
	JAK/Stat Signaling		A	A							A
	mTOR Signaling										A
	p38 MAPK Signaling	A	A		A				A	A	A
	PDGF Signaling		A	A			A				
	PI3K/AKT Signaling	A	A	I	A		A	A		A	A
	RhoA Signaling	A	A				A				
	Signaling by Rho Family GTPases	A	A				A				A
	STAT3 Pathway		A		A		A				A
	TGF-β Signaling		A		A		A				
	VEGF Family Ligand-Receptor Interactions			A							A
	VEGF Signaling		A				A				A
	Wnt/β-catenin Signaling										
ECM	Inhibition of Matrix Metalloproteases		I	A		I					
	Integrin Signaling		A				A				A
Inflammation	Chemokine Signaling		A	I			A				
	Dendritic Cell Maturation	A	A						A	A	A
	HMGB1 Signaling	A	A		A	A	A			A	A
	IL-1 Signaling									A	A
	IL-2 Signaling						A				
	IL-4 Signaling			A							
	IL-6 Signaling	A	A		A				A	A	A
	IL-7 Signaling Pathway			A							A
	IL-8 Signaling	A	A		A	A	A		A	A	A
	IL-9 Signaling										
	IL-10 Signaling										
	IL-12 Signaling and Production in Macrophages										
	IL-15 Signaling										
	IL-17 Signaling										
	IL-17A Signaling in Fibroblasts										
	iNOS Signaling	A	A			A					A
	Interferon Signaling					A		A			
	LPS/IL-1 Mediated Inhibition of RXR Function		A		A						
	LPS-stimulated MAPK Signaling	A					A	A		A	A
	T Cell Receptor Signaling			A							
	Th1 and Th2 Activation Pathway										
	Toll-like Receptor Signaling		A		A	A			A		A
Cell cycle and apoptosis	Apoptosis Signaling										I
	Cell Cycle Control of Chromosomal Replication										
	Cell Cycle Regulation by BTG Family Proteins		A	A							
	Cell Cycle: G1/S Checkpoint Regulation			A	A						
	Cell Cycle: G2/M DNA Damage Checkpoint Regulation			A	A						
	Cyclins and Cell Cycle Regulation				I			A			I
	Death Receptor Signaling	A				A		A			
	HIPPO signaling			A							
	Myc Mediated Apoptosis Signaling			A							
	NF-κB Signaling		A	A	A		A		A		A
	p53 Signaling										
Hypoxia ROS	HIF1α Signaling										
	Mitochondrial Dysfunction										
	NRF2-mediated Oxidative Stress Response		A	A	A	A		A			A
	Oxidative Phosphorylation	I	I	A	I			I			I
Other	Atherosclerosis Signaling			A							
	Osteoarthritis Pathway		A	I	A	A	A	A	A	A	A
	PPAR Signaling	I	I	I	I	I	I	I	I	I	I
	PPARα/RXRα Activation	I	I		I		I	I	I		I
	RANK Signaling in Osteoclasts						A				A
	Renin-Angiotensin Signaling										A
	Osteoblasts, Osteoclasts and Chondrocytes in Rheumatoid Arthritis										

of the *z*-score showed only activation as the direction of change. The organ with the most activated pathways was colon (9 out of 22). Some pathways such as dendritic cell maturation, HMGB1, IL-6, IL-8 signalling and LPS-stimulated MAPK signalling showed activation for three or four human organs PCTS.

Other pathways

Furthermore, our analysis also included pathways related to cell cycle and apoptosis, hypoxia and oxidative stress, metabolism and degenerative disorders. Amongst murine organs, colon PCTS had the lowest number of significantly changed pathways, whereas kidney PCTS had the highest. In contrast, human liver and jejunum PCTS had the lowest number of significantly changed pathways and colon PCTS had the most. The pathways that showed significant change in all murine and human PCTS were HIF1α signalling, osteoarthritis pathway, role of osteoblasts, osteoclasts and chondrocytes in rheumatoid arthritis. Pathway activation was observed for NF-κB signalling, NRF2-mediated oxidative stress response and osteoarthritis pathway in both species. Moreover, PPAR signalling and PPARα/RXRα activation showed inhibition as the direction of change also in both species.

Differences and similarities in regulation of selected pathways in murine and human PCTS

The preselected pathways showed species and organ-specific changes during PCTS culture. In murine PCTS, ileum and colon PCTS had the lowest number of significantly changed pathways during culture, while kidney had the highest. However, we obtained different results for human PCTS: jejunum PCTS had the lowest number of significantly changed pathways during culture, whereas colon PCTS had the highest. As for direction of change, most of the preselected pathways were activated in both species. For an organ-specific comparison between murine and human PCTS, we used a four set Venn diagram (Heberle et al. 2015) with the following sets for mouse—significant *p* value (group A, pathways with p value ≤ 0.01) and *z*-score (group B, activated or inhibited, $|z\text{-score}| \geq 2$), and human—significant *p* value (group C) and *z*-score (group D) (Fig. 8). The table shows the common pathways between the species (ABCD), together with species-specific pathways (AB for mouse and CD for human). The pathways included in all other groups in Venn diagram are provided in File S4. The intersection of the four data sets (ABCD in Fig. 8) showed that after PCTS culture, there were two common fibrosis pathways: PI3K/AKT signalling (liver and kidney) and p38 MAPK signalling (ileum). These intersections included also inflammation-related pathways: HMGB1 signalling (liver, colon), IL-6 signalling (ileum), IL-8 signalling (liver, ileum, colon) and LPS-stimulated MAPK signalling (liver). Other common pathways were osteoarthritis pathway (kidney, jejunum, ileum and colon), NRF-2-mediated oxidative stress response (kidney and colon) and PPAR signalling (jejunum and ileum). Regarding species-specific pathways, among murine organs, kidney PCTS displayed most of the differences, which included especially fibrosis and inflammation-related pathways. However, amongst human organs, colon PCTS showed the largest number of species-specific pathways (17). Beside the top most significantly changed pathways, IPA allows the analysis of certain pathways of interest. We showed the changes in preselected canonical pathways during PCTS culture that had organ and species differences in their regulation.

Discussion

Drug development is a long and expensive process. The attrition rates of clinical trials are high although extensive advances were made in biomedical research, such as the sequencing of the human genome, in silico drug target identification (Kim et al. 2017) and in vitro assessment of pharmacological properties (absorption, distribution, metabolism and excretion) for new chemical compounds. One of the reasons for this is inadequate preclinical development, which includes in vivo, in vitro and ex vivo models that try to bridge the gap between the bench and the clinic. To increase the success rate of preclinical studies, often hampered by the use of animal models lacking translational power, human predictive models that are relevant to the research question are preferred. An emerging model is represented by precision-cut tissue slices (PCTS)—a complex ex vivo system that preserves organ architecture and cell–cell interactions, and allows the use of human tissue. In Part I of this study, we described the changes in the transcriptional profiles during culture of PCTS obtained from five different healthy organs (liver, kidney, jejunum, ileum and colon) and two species (mouse and human). Our goal was to identify shared and differential regulators that mediate the changes in PCTS during culture, as a first step towards the validation of the model.

PCTS preparation and culture entail (cold) ischemia during organ collection, mechanical stress due to slicing and induction of biological processes as a result of 48-h culture. The biological processes induced in cultured PCTS were characterized by extensive transcriptional changes reflected by the high number of up/downregulated differentially expressed genes (DEGs). The regulation profiles of murine and human PCTS were driven mostly by organ type and time in culture, as shown by PCA (Fig. 2a–d). An interesting difference between the two species was observed in the clustering of intestinal samples after culture. Mouse jejunum and ileum PCTS clustered together, followed by clustering

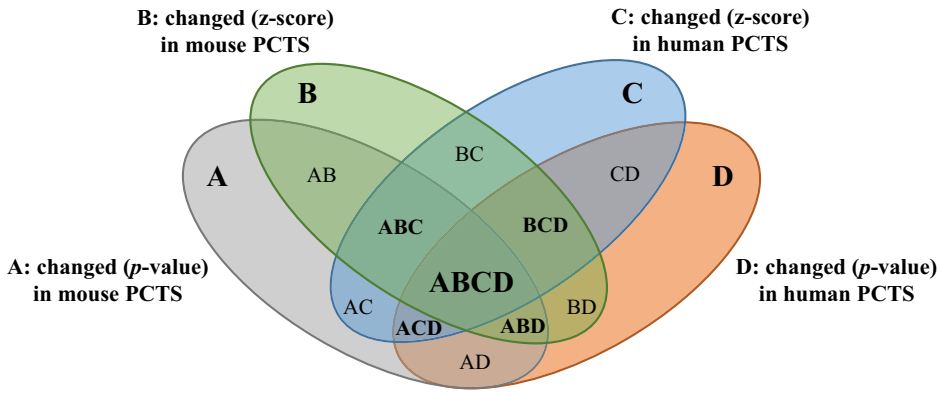

Group	Liver PCTS	Kidney PCTS	Jejunum PCTS	Ileum PCTS	Colon PCTS
ABCD	PI3K/AKT Signaling HMGB1 Signaling IL-8 Signaling LPS-stimulated MAPK Signaling	PI3K/AKT Signaling NRF2-mediated Oxidative stress response Osteoarthritis Pathway	Osteoarthritis Pathway PPAR Signaling	p38 MAPK Signaling IL-6 Signaling IL-8 Signaling Osteoarthritis Pathway PPAR Signaling	HMGB1 Signaling IL-8 Signaling NRF2-mediated Oxidative stress response Osteoarthritis Pathway
AB	Dendritic Cell Maturation IL-6 Signaling iNOS Signaling Death Receptor Signaling Oxidative Phosphorylation	BMP signaling pathway JAK/Stat Signaling p38 MAPK Signaling PDGF Signaling RhoA Signaling TGF-β Signaling VEGF Signaling Chemokine Signaling Dendritic Cell Maturation iNOS Signaling LPS/IL-1 Mediated Inhibition of RXR function Toll-like Receptor Signaling NF-κB Signaling	VEGF Family Ligand-Receptor interactions T Cell Receptor Signaling	STAT3 Pathway LPS/IL-1 Mediated Inhibition of RXR function NF-κB Signaling	-
CD	PDGF Signaling	Cyclins and Cell Cycle Regulation	-	IL-1 Signaling LPS-stimulated MAPK Signaling	BMP signaling pathway ERK/MAPK Signaling HGF Signaling JAK/Stat Signaling mTOR Signaling PI3K/AKT Signaling VEGF Family Ligand-Receptor interactions IL-1 Signaling LPS-stimulated MAPK Signaling Apoptosis Signaling Cyclins and Cell Cycle Regulation NF-κB Signaling Oxidative Phosphorylation PPARα/RXRα Activation RANK Signaling in Osteoclasts Renin-Angiotensin Signaling

Fig. 8 Four-set Venn diagram illustrating significantly changed selected pathways in murine and human PCTS. Canonical pathways in group ABCD are significantly changed (based on *p* value and *z*-score) during culture pathways in both murine and human PCTS, whereas pathways in groups AB and CD are signalling pathways significantly changed only in murine PCTS (AB) or only in human PCTS (CD). Full list of pathways included in rest of the groups is provided in File S4

with colon PCTS. This was expected as jejunum and ileum are part of the small intestine and share more features than with colon. However, human intestine PCTS showed distinct clustering, with ileum being more similar to colon than jejunum. This may be explained by the cellular composition of human intestinal PCTS: their preparation includes the removal of the submucosa, muscularis and serosa due to the thickness and stiffness of these components. Additionally, human jejunum PCTS have the smallest number of changed transcripts (hundreds vs. thousands in the other organs), indicating that slices of gut mucosa were less affected by culture than the other organs. Next, we observed that liver and kidney PCTS clustered based on species and not organ of origin (Fig. 2e), indicating that although these two organs have very different cellular composition, the culture-induced processes were species specific.

We investigated the top regulated genes to identify the common modulators that drive the changes during culture in each organ. Although most transcripts were organ specific, *IL11*, *MMP3* and *MMP10* were commonly present among top upregulated DEGs in murine and human PCTS. These common markers show that culture produces a similar biological response in human and murine PCTS. IL-11 is an anti-inflammatory cytokine that has a direct effect on macrophages by reducing the production of IL-1β, IL-12, nitric oxide and NF-κB (Schwertschlag et al. 1999).

Additionally, IL-11 is also involved in the repair response by promoting fibroblast activation across different organs and species (Schafer et al. 2017). MMPs represent a group of enzymes with various functions in biological processes, such as inflammation, injury, tissue repair and remodelling (Parks et al. 2004); therefore, it was likely to have them in the top regulated transcripts. MMP3 (stromelysin-1) and MMP10 (stromelysin-2) are secreted by fibroblasts and epithelial cells and have different function in immunity and wound healing (Page-McCaw et al. 2007), such as activation of IL-1β, MMP9 and certain collagenases (Overall 2002; Barksby et al. 2006; Geurts et al. 2008).

To deepen our understanding of the culture-induced condition, we used IPA to decipher the NGS-derived data. IPA revealed activation of inflammatory pathways in all organs from both species, indicating that culture induces a non-specific inflammatory response. The most common inflammatory pathways across organs and species were IL-6, IL-8 signalling, high mobility group box 1 (HMGB1) signalling, LPS/IL-1-mediated inhibition of RXR function and acute phase response signalling. Damaged or dying cells, resulting from non-infectious inflammation caused by mechanical stress or apoptosis/necrosis, release several damage-associated molecular patterns (DAMPs). Representative examples for DAMPs are mitochondrial DNA, which can lead to Toll-like receptor (TLR) 9 stimulation and NF-κB activation (Zhang et al. 2010), as well as HMGB1, an agonist of TLR2 and TLR4 (Sims et al. 2010). The effect of DAMPs on macrophages, fibroblasts and endothelial cells will result in an immune response characterized by the release of pro-inflammatory cytokines and chemokines: TNF-α, IL-1α/β, IL-6, IL-8 and MCP1, growth factors and ECM-degrading enzymes (MMPs) (Zhong et al. 2009; Piccinini and Midwood 2010; Sims et al. 2010; Yu et al. 2019). In our study, we observed increased mRNA levels for these pro-inflammatory molecules in PCTS during culture; however, it has to be further elucidated whether these changes translate into changes on protein level.

The increased expression of growth factors and MMPs shows that the non-specific defense mechanism is coupled with tissue repair processes. Two pathways characterized by inflammation and tissue remodelling were enriched in all organ PCTS (osteoarthritis pathway and role of osteoblasts, osteoclasts and chondrocytes in rheumatoid arthritis) (Gierut et al. 2010; Bar-Or et al. 2015). Considering that the studied PCTS do not have chondrocytes, osteoclasts or osteoblasts, we presume that the fibroblasts and organ-resident immune cells are responsible for the transcripts encoding immune mediators and metalloproteases (MMPs and ADAMTs) that activate these pathways.

On the other hand, culture resulted in the inhibition of many canonical pathways, especially those involved in biosynthesis, endogenous metabolism and transport. This indicates the reduction of the enzymatic and metabolic activities in PCTS after 48 h. In contrast, previous microarray study on human liver PCTS showed that 24-h incubation has led only to small changes in the expression of genes involved in metabolism and drug transport (Elferink et al. 2011). Given these points, we consider that most changes occur in the second half of the 48-h culture and this has to be taken into consideration for studies related to absorption, metabolism and excretion in different organs. In particular, two pathways were commonly inhibited in mouse and human organs: PPAR signalling and LXR/RXR activation. These are the pathways of nuclear transcription factor receptors: peroxisome proliferator-activated receptor (PPAR), liver X receptor (LXR) and retinoid X receptor (RXR) and have a role in cellular metabolism. The inhibition of PPAR signalling in PCTS might be caused by the high concentration of glucose in the culture media (25 mM), as similar concentrations of glucose were reported to inhibit PPAR (Roduit et al. 2000; Cheng et al. 2013; Domínguez-Avila et al. 2016) and to lead to several transcriptional changes in different organs (Katsoulieris et al. 2016; Boztepe and Gulec 2018). However, further functional experiments are needed to confirm this hypothesis. The inhibition of PPAR signalling leads to a reduction in β-oxidation of fatty acids, which can cause an accumulation of fatty acid anions in the mitochondria (Ho et al. 2002). As a result, the excess lipids inhibit the respiratory complexes of the electron transport chain in the mitochondria. This may lead to mitochondrial dysfunction, decreased ATP, production of reactive oxygen species, inflammation and necrosis (Fromenty and Pessayre 1995; Wajner and Amaral 2016). The inhibition of PPAR signalling was supported by the inhibition of the oxidative phosphorylation pathway and activation of NRF-2-mediated oxidative stress response. The oxidative phosphorylation pathway represents the mitochondrial production of ATP from the electron transport system, and its inhibition is reflected by a decrease in ATP. In turn, NRF-2-mediated oxidative stress response regulates the damage induced by oxidative stress (Ma 2013). The second common inhibited pathway was LXR/RXR activation, which is also involved in lipid metabolism and cholesterol to bile acid catabolism (Murthy et al. 2002). This pathway can be inhibited as a result of TLR4 activation (Kidani and Bensinger 2014), receptor responsive to HMGB1, as previously mentioned. These changes show the decline of lipid metabolism during PCTS culture.

Activation of NRF-2-mediated oxidative stress response pathway and HIF1α signalling in PCTS during culture is likely to be associated with exposing the PCTS to high oxygen levels (80%) for 48 h. Given that each slice is about ten cell layers thick (approx. 250 µm), high concentration of oxygen is necessary to ensure its diffusion from culture medium into the deep inner cell layers. It has been shown

that oxidative stress plays an important role in fibrosis development (Poli 2000; Liu and Gaston Pravia 2010; Lv et al. 2018). Therefore, induction of oxidative stress and activation of the hypoxia-related signalling pathways in PCTS could be perceived as an advantage of this ex vivo fibrosis model.

IPA can identify the changes in hundreds of signalling pathways, together with the prediction for the direction of the downstream effects of different biological processes. To better visualize the intricacies in culture of different organs PCTS from two species, we focused on a number of pathways related to inflammation and fibrosis (Fig. 7), as previous studies reported a fibrogenic process during PCTS culture (Stribos et al. 2016; Westra et al. 2016; Luangmonkong et al. 2017). For each pathway, we showed two statistical parameters: the *p* value and the *z*-score. Both parameters are important to identify the significance of the pathways that are driving the biological processes and the regulators of interest. We observed significant changes in the pathways that drive inflammation and fibrosis (Wynn 2008), corroborating the use of PCTS as a tool for studying antifibrotic drugs. As an illustration, fibroblasts, which upon activation promote intense tissue remodelling, can be induced in our system by several pathways and mediators, such as TGFβ–STAT3 pathway (Chakraborty et al. 2017), TLR activation (Bhattacharyya et al. 2017), chemokines (Sahin and Wasmuth 2013) (e.g. gene encoding CCL2 is upregulated during culture in both species and all organs except jejunum), and inhibition of PPAR signalling (Mann et al. 2010). Additionally, the number of fibroblasts can increase as a result of epithelial or endothelial cell–mesenchymal transition or activation of resident cells, such as hepatic stellate cells in liver. Collectively, focusing the analysis on certain pathways helps answering a specific research question, especially when more groups are compared (several organs and species).

A major advantage of the PCTS system is the possibility to use human tissue, eliminating the need for mouse–man translation. Our results further emphasize just how important the use of human tissue is in pharmacological research, as majority of identified DEGs were regulated differently in mouse and human PCTS during culture. However, preclinical studies performed on laboratory animals remain a critical requirement for drug development. Therefore, it is crucial to identify both common and species-specific regulated canonical pathways in murine and human PCTS when investigating a certain pathway or pathology. Considering that inflammation and fibrosis represent our main interests, we used a 4-set Venn diagram (Fig. 8) on selected pathways to identify the shared and unique pathways between the two species for each organ PCTS. The species-specific pathways give an indication of the interspecies differences during culture and can hint for which targets the mouse is not the suitable research animal. However, we have to take into consideration that although culture is a process characterized by an acute inflammatory response, infiltrating blood-derived immune cells are not present, resulting in a different state than the in vivo situation.

One of the disadvantages of PCTS is the limited incubation time due to the loss of tissue viability. The understanding of biological processes that occur in PCTS during culture gives us the possibility to suggest strategies for culture optimization. For instance, the inflammatory process in PCTS can be reduced with specific compounds that decrease the expression of inflammatory cytokines [e.g. prednisolone (Heimburger et al. 2000)] or inhibit other factors involved in inflammation [e.g. parthenolide inhibits NF-κB (Mathema et al. 2012)]. Of note, the profibrotic response observed in slices might diminish upon the reduction of inflammatory response, as it is shown by Iswandana et al. in murine intestinal PCTS treated with rosmarinic acid (Iswandana et al. 2016). Next, reduced lipid metabolism in PCTS during culture might be improved if the function of PPARα/δ is restored using the agonist elafibranor (Ratziu et al. 2016) that increases the β-oxidation of fatty acids. This could be of particular interest for liver PCTS as they can be used for preclinical studies of non-alcoholic liver disease, a condition characterized by excess lipid accumulation. Next, mitochondrial function could be better preserved if the culture media is supplemented with compounds that have a positive effect on the mitochondria, such as α-lipoic acid (Shay et al. 2009), L-carnitine (Marcovina et al. 2013) or coenzyme Q10 (Orsucci et al. 2011). Lastly, we recommend adding fatty acids and insulin in physiological concentrations to the culture media. Fatty acids (e.g. essential linoleic and linolenic acids) could stimulate the inhibited pathways involved in lipid metabolism, whereas insulin has several roles in both carbohydrate and lipid metabolisms (Dimitriadis et al. 2011). The suggested methods of culture optimization might lead to prolonged viability, which is a necessary aspect for the validation of the method. It has to be noted that these factors, when added to the culture medium, might influence the expression of genes and proteins in PCTS. While the same holds true for the antibiotics that were added to Williams' medium E for culturing any organ PCTS to prevent microbial contamination, there is little evidence that these compounds impact the transcription of fibrosis- and inflammation-related genes.

Part II: Characterization of diseased human precision-cut tissue slices in culture and their comparison to healthy control slices

Results of Part II

In Part II of this study, we investigated transcriptional changes in human PCTS by RNA sequencing. Figure 9a shows the general workflow. PCTS obtained from clinically healthy control tissues from patients with various underlying diseases will be further addressed as "healthy PCTS". In turn, PCTS obtained from patient diseased (fibrotic) tissues will be termed "diseased PCTS". PCTS were prepared from human healthy and diseased tissues, namely liver, kidney and ileum, and cultured for 48 h. Of note, human lung slices were prepared as described in "Methods", but hereafter were excluded from the downstream analyses since diseased lung tissue was available only from one patient and no healthy lung tissue could be obtained. PCTS were collected at 0 h and 48 h, which were then used for viability measurement and deep sequencing. Additionally, culture medium after 24 h and 48 h was used for secreted cytokines detection. All tissue slices remained viable after 48 h culture (Fig. S10a). Although jejunum and ileum PCTS had lower RNA quality compared to RNAs from liver and kidney PCTS, the overall RNA sample quality was good, with mean RNA integrity numbers > 7. There was no systematic difference with respect to RNA quality between samples from diseased vs. healthy PCTS. Interestingly, we observed a slight increase in RNA integrity numbers in 48 h samples compared to 0 h samples (data not shown). Total number of sequenced reads varied between 25 and 75 million reads per sample, with an average of 61 million reads. Alignment statistics indicated that the data were of high quality and provided sufficient sequencing depth to pursue differential expression testing between the experimental groups. For instance, the mean rate of unique-mapping exonic reads was 62% per sample.

(IIa) Principal component analysis and hierarchical clustering in human PCTS

Figure 9b illustrates the results from the PCA derived from all genes with scatter plots of the first three components PC1, PC2 and PC3 that explained together almost 50% of the observed variance in the data. Generally, there was a consistent clustering of the samples by tissue type (liver, kidney and ileum) in PC1 and by culture time in PC2 (0 h and 48 h). Interestingly, these strong tissue- and culture time-dependent effects superimposed differences between diseased and healthy PCTS since there was no clear separation of the samples by pathology in the first three components. Percentages of explained variance for each of the first three principal components are indicated in Fig. S2c, d, which illustrates PCA results for all analysed human PCTS (healthy and diseased), including human fibrotic lung slices. The latter were excluded from the downstream analyses because diseased lung PCTS were obtained from only one patient, and healthy control lung tissue was unavailable. In line with PCA results, hierarchical clustering showed stronger separation of human PCTS by tissue type than by pathology or culture time (Fig. 9c, d).

Figure 10 outlines the main directions of performed analyses to aid the general understanding of the study concept.

(IIb) Transcriptomic characterization of human diseased PCTS

Genes differentially expressed in diseased PCTS during culture

While in Part I we performed a comprehensive transcriptomic analysis of human healthy PCTS, in Part II, we provide a characterization of human PCTS prepared from diseased tissues by describing the transcripts and pathways that were affected by culture (Fig. 11). Generally, we identified a large number of differentially expressed genes (DEGs) during 48 h culture in all PCTS. In particular, we found 4808 DEGs in diseased liver PCTS, 3037 DEGs in kidney and 1138 DEGs in ileum PCTS (Fig. 11a; volcano plots in Fig. S10b). Regarding the directionality of change, we found that nearly half of all DEGs were upregulated in kidney and ileum PCTS, whereas 64% of transcripts in liver were downregulated during culture. The complete lists of DEGs (p_{adj} value ≤ 0.01 and $\log_2$ (FC) ≥ 1) in diseased PCTS are provided in File S5.

Top regulated genes and enriched pathways in diseased PCTS during culture

To gain better insight into culture-induced changes in diseased PCTS, we identified strongly regulated genes (based on fold change) during 48 h of culture, and selected top ten genes (up- and downregulated) that showed highest significant changes in their expression (Fig. 11b). Transcripts were ranked based on the absolute $\log_2$ (FC) values, and their descriptions are provided in Table S5. The top ten most upregulated genes in diseased PCTS during culture often included genes related to inflammation (*IL11, SERPINB2, IL13RA2, CHI3L1*), proteases involved in ECM organization (*MMP1, MMP3, MMP10*) and transporters (*SLC7A11, CLCA4*). *MMP1*, the gene that encodes interstitial

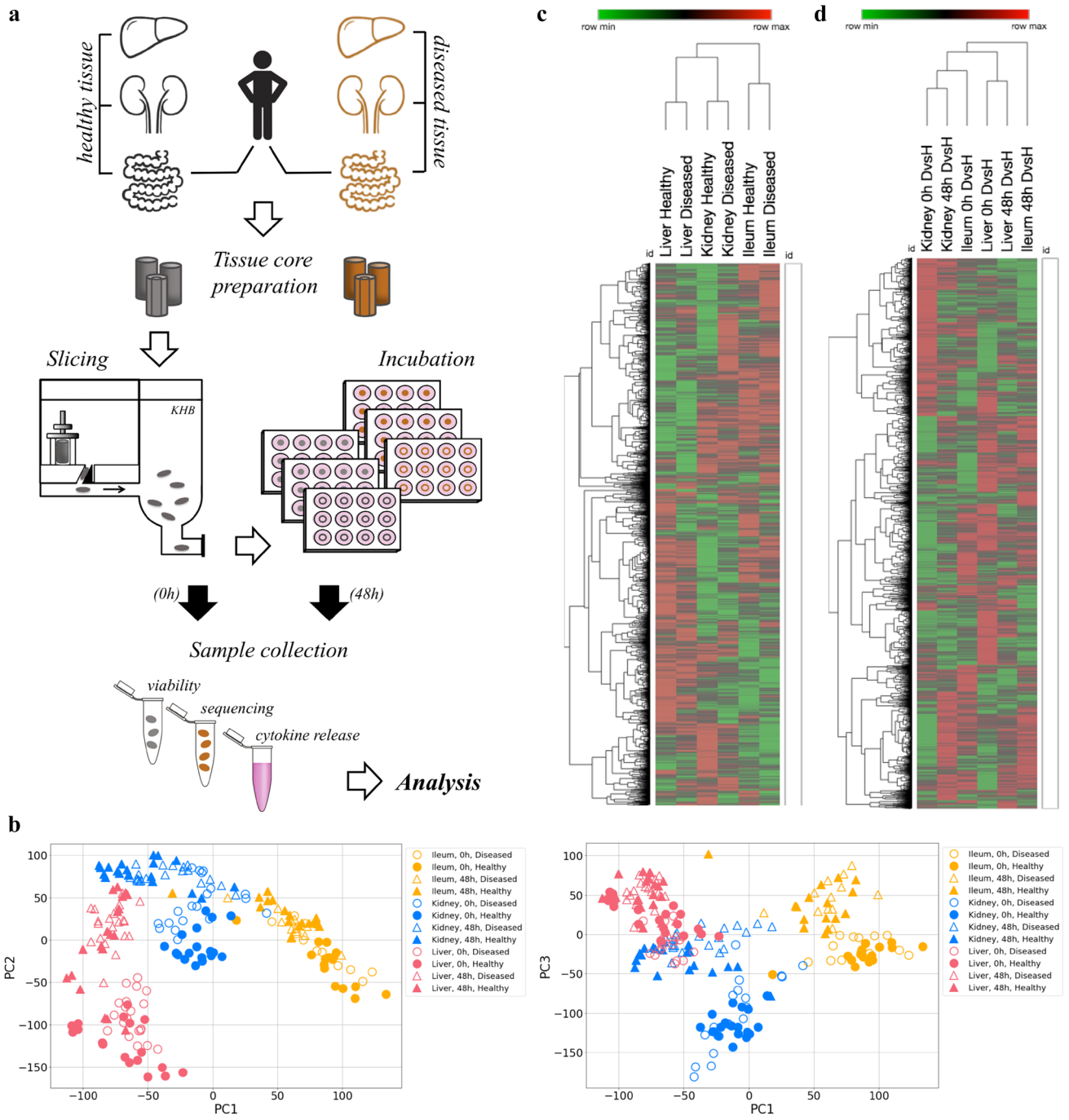

Fig. 9 Study workflow, principal component analyses (PCA) and hierarchical clustering in human healthy and diseased PCTS. **a** Precision-cut tissue slices (PCTS) were prepared from human healthy or diseased liver, kidney and ileum using Krumdieck tissue slicer and incubated for 48 h. Samples were collected at 0 h (prior incubation) and at 48 h for viability measurement, sequencing analysis and cytokine release in the culture medium. **b** Scatter plots of the dimensions PC1 vs. PC2 and PC1 vs. PC3. Samples are coloured by tissue type, shaped by incubation time (0 h or 48 h) and colour filled by pathology (healthy or diseased). The heatmap of $\log_2$ (FC) values illustrates expression of 18,667 genes (with $p_{adj} \leq 0.01$) in human healthy and diseased PCTS during culture (**c**) and in pairwise comparisons diseased vs. healthy PCTS at 0 h vs. 48 h (**d**). Independent clustering analysis shows stronger separation of samples by tissue type (liver, kidney and ileum) than by pathology or culture time (colour figure online)

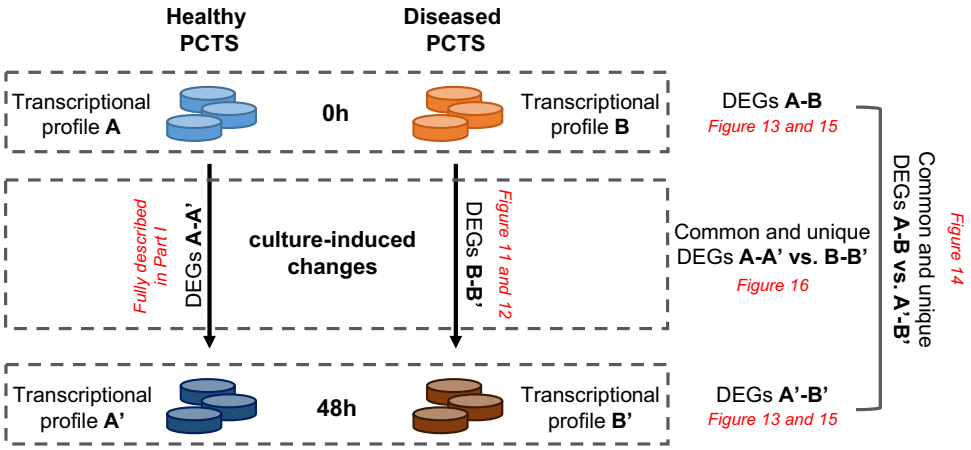

Fig. 10 Visual summary of the study, capturing the concept and main lines of performed analysis. Human healthy PCTS (**a**) undergo substantial transcriptional changes during 48-h culture and acquire profile A', with thousands of genes differentially expressed between A and A'. These culture-induced DEGs (DEGs A–A') and involved canonical pathways are described in detail in Part I. Similarly, diseased PCTS (**b**) are also profoundly affected by culture, as they display thousands of DEGs (DEGs B–B'), and develop 48-h transcriptional profile B'. We compared the impact of culture on healthy and diseased PCTS by uncovering differences and similarities between data on DEGs A–A' (top transcripts and canonical pathways) presented in Part I and DEGs B–B' described in Part II. We also determined common and unique transcripts between culture-induced DEGs in healthy slices (A–A') and in diseased slices (B–B'). Based on common DEGs A–A' vs. B–B', we identified biological pathways commonly changed in healthy and diseased PCTS

collagenase, was the only common gene between the top ten DEGs in all three organs and it was the highest or second highest upregulated gene during 48-h culture. On the other hand, genes encoding enzymes (*PCK1, HAO2, ACSM2A, ACSM2B, NAT8, FMO, GLYAT*), transporters (*SLC13A1, SLC5A12, SLC34A1*) and molecules involved in the immune response (*CXCR1, FCGR2B, ACKR1*) represented the top of the downregulated genes.

Next, to assess which biological pathways are involved in the culture of diseased PCTS, we performed IPA on all DEGs from diseased liver, kidney and ileum PCTS. We identified significantly changed canonical pathways (with a p value ≤ 0.01) that also showed a direction of change based on a z-score ≥ 2 (predictor of activation) or ≤ -2 (predictor of inhibition). The top five most activated and the top five most inhibited canonical pathways in diseased human PCTS during culture are displayed in Fig. 11c. Complete lists of significantly changed pathways (provided in Fig. S11) revealed that osteoarthritis pathway was activated in all diseased PCTS. Despite its name, osteoarthritis pathway involves numerous fibrosis- and inflammation-related genes (see "Discussion" of Part II). Three pathways—actin nucleation by ARP–WASP complex, integrin signalling and ephrin receptor signalling—were commonly activated in liver and kidney PCTS, whereas acute phase response signalling was present in both kidney and ileum PCTS. Moreover, diseased kidney and ileum PCTS shared culture-induced activation of other four pathways that were related to cholesterol biosynthesis. Among commonly inhibited pathways, LXR/RXR activation was found in all cultured organ PCTS. Furthermore, after 48 h in culture several metabolism-related pathways were inhibited (for example, nicotine, melatonin, serotonin and tryptophan degradation) in liver and kidney PCTS.

Regulation of fibrosis- and inflammation-associated pathways in diseased PCTS during culture

Culturing of healthy slices results in the development of spontaneous (i.e. not exogenously induced) fibrogenic and inflammatory responses; however, little is known about the impact of culture on slices prepared from diseased tissues. Considering that the Ingenuity Pathways Knowledge Base (IPKB) contains information on more than 330 biochemical pathways, we selected several canonical pathways a priori, with a focus on fibrosis and inflammation, and investigated their regulation in diseased PCTS. Figure 12 illustrates the culture-induced changes in the selected pathways in diseased PCTS (information on key signalling molecules involved in each pathway is provided in File S3). Fibrosis-associated signalling pathways showed significant changes in all PCTS, especially in liver PCTS, where 12 out of 17 canonical pathways were altered at 48 h. Kidney and ileum showed less changes: only three pathways were regulated significantly different at 48 h compared to 0 h. The direction of change (indicated by the z-score) showed activation of PI3K/AKT signalling in liver and kidney, whereas this pathway was inhibited in ileum PCTS. Additionally, liver PCTS displayed activation of BMP signalling and STAT3 pathway, and p38 MAPK

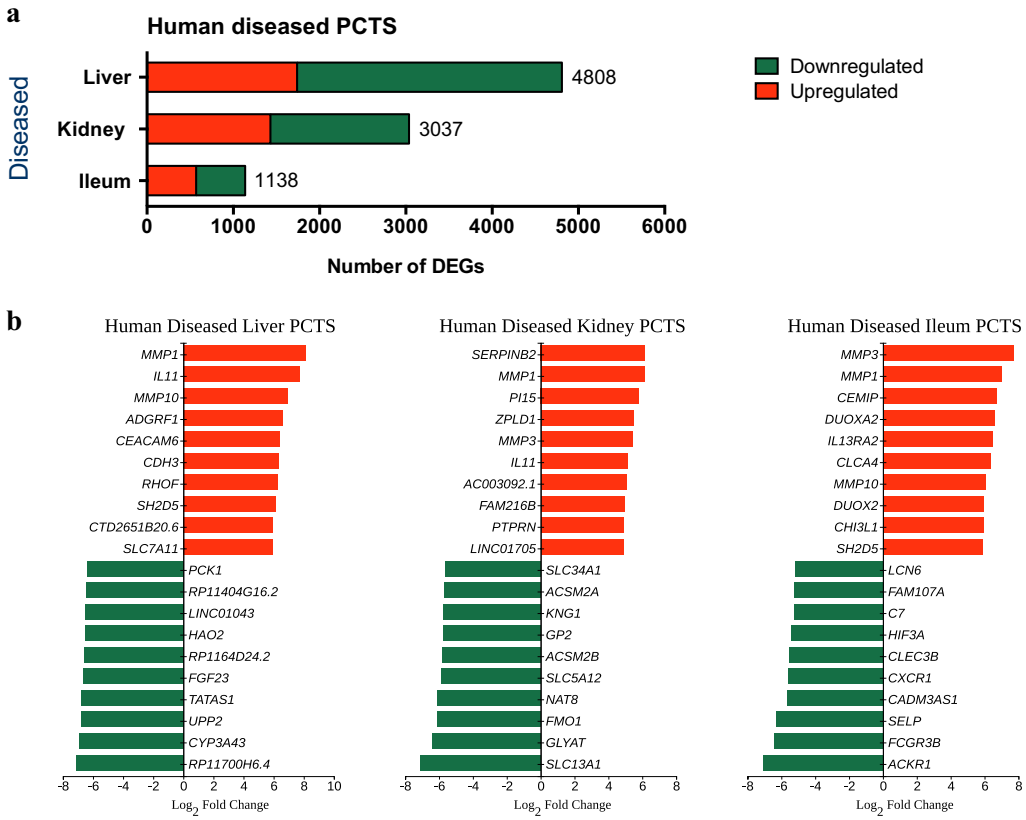

c

		Canonical Pathway	z-score	-log(p-value)	Size	Downregulated (%)	Upregulated (%)	Overlap (%)
Activated	Liver	PI3K/AKT Signaling	3,02	3,19	131	20	56	76
		LPS/IL-1 Mediated Inhibition of RXR Function	2,97	23,10	222	56	27	84
		Ephrin Receptor Signaling	2,72	5,18	179	26	54	80
		Actin Nucleation by ARP-WASP Complex	2,71	5,11	62	16	60	76
		p53 Signaling	2,35	4,36	111	32	47	79
	Kidney	Actin Nucleation by ARP-WASP Complex	3,50	3,12	62	23	53	76
		Osteoarthritis Pathway	3,33	3,74	212	31	49	80
		Integrin Signaling	2,60	4,04	219	26	48	75
		Superpathway of Cholesterol Biosynthesis	2,33	2,67	28	21	64	89
		Acute Phase Response Signaling	2,27	2,89	176	31	52	82
	Ileum	Osteoarthritis Pathway	3,40	5,94	212	26	54	80
		Superpathway of Cholesterol Biosynthesis	3,32	7,81	28	11	79	89
		NRF2-mediated Oxidative Stress Response	2,71	3,16	199	24	50	74
		Colorectal Cancer Metastasis Signaling	2,60	3,66	254	26	52	78
		Cholesterol Biosynthesis I	2,45	4,97	13	8	92	100
Inhibited	Liver	Nicotine Degradation II	-5,66	9,72	65	65	11	75
		Melatonin Degradation I	-5,48	8,31	65	68	11	78
		Nicotine Degradation III	-5,20	8,06	56	64	13	77
		LXR/RXR Activation	-5,17	22,50	121	67	27	94
		Superpathway of Melatonin Degradation	-5,15	10,10	70	67	13	80
	Kidney	PPAR Signaling	-2,98	2,24	101	20	54	74
		iCOS-iCOSL Signaling in T Helper Cells	-2,52	2,17	123	46	28	75
		Tryptophan Degradation III (Eukaryotic) (*)	-2,12	2,42	25	60	36	96
		LXR/RXR Activation (*)	-2,07	2,26	121	43	50	94
		Serotonin Degradation (*)	-2,00	2,10	77	61	16	77
	Ileum	Cyclins and Cell Cycle Regulation	-2,83	2,47	81	41	36	77
		LXR/RXR Activation (*)	-2,71	3,45	121	31	62	94
		Antioxidant Action of Vitamin C	-2,65	2,94	108	31	47	81
		Estrogen-mediated S-phase Entry	-2,65	3,94	26	62	19	81
		Mitotic Roles of Polo-Like Kinase	-2,12	3,16	66	38	35	73

Fig. 11 Characterization of human diseased PCTS. **a** Total number of differentially expressed genes (DEGs), upregulated and downregulated, in human diseased PCTS. DEGs were defined as genes with $\log_2$ (FC) ≥ 1 and p_{adj} value ≤ 0.01. Full lists of identified DEGs are provided in File S5. **b** Top ten regulated DEGs based on the $\log_2$ (FC) values. Gene descriptions are provided in Table S5. **c** Top five canonical pathways identified by IPA. Only pathways with p value ≤ 0.01 and a z-score ≥ 2 (predictor of activation) or ≤ -2 (predictor of inhibition) were included. Pathway size (i.e. total number of genes in a pathway), percentage of significantly downregulated (green bars) and upregulated (red bars) genes in a given pathway, and percentage of overlap with the dataset (grey bars) are indicated for each pathway. Full lists of significantly changed pathways in PCTS from each organ are provided in Fig. S11 (colour figure online)

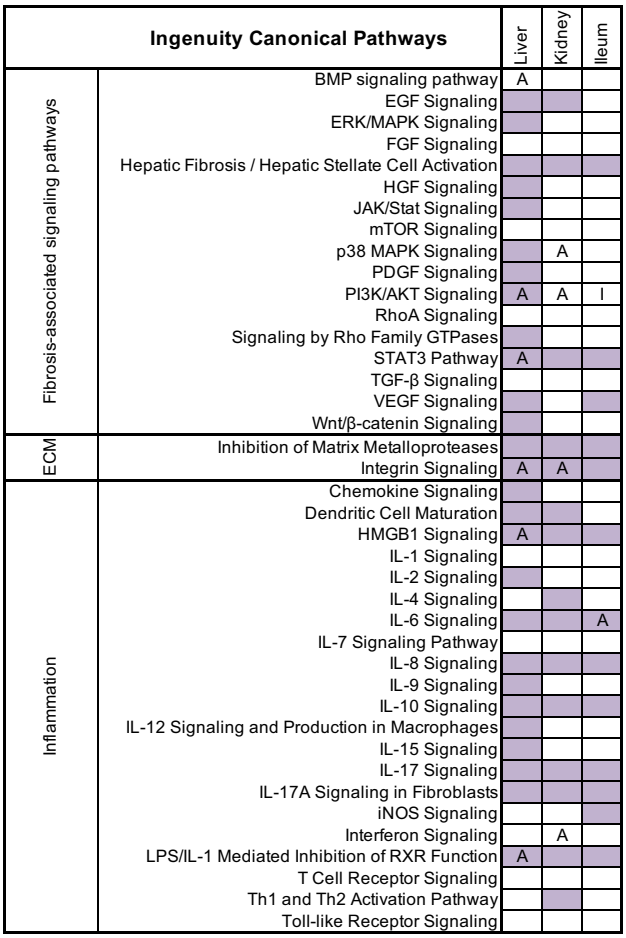

Fig. 12 Regulation of preselected pathways in human diseased PCTS during 48-h culture. Purple colour indicates a significant pathway change based on a p value ≤ 0.01, whereas predicted pathway activation (A) or inhibition (I) is indicated by a z-score, if available. Signalling molecules involved in each preselected pathway are shown in File S3 (colour figure online)

signalling was activated in kidney PCTS. Furthermore, two selected canonical pathways related to ECM organization, namely inhibition of matrix metalloproteases and integrin signalling, showed significant culture-induced changes in PCTS from all diseased organs. Activation was predicted only for integrin signalling in liver and kidney.

Similarly, inflammation-associated pathways also showed significant changes in all diseased PCTS after 48 h culture: out of 21 selected pathways, culture altered 13 pathways in liver PCTS, 11 in kidney PCTS and 8 in ileum PCTS. In addition, seven of these changed pathways were affected by culture in all three organs and included HMGB1 signalling, IL-6, IL-8, IL-10, IL-17 signalling, IL-17A signalling in fibroblasts and LPS/IL-1-mediated inhibition of RXR function. The only predicted direction of change was the activation of HMGB1 signalling and LPS/IL-1-mediated inhibition of RXR function in liver PCTS, interferon signalling in kidney PCTS, and IL-6 signalling in ileum PCTS.

Overall, culture induced significant changes in fibrosis- and inflammation-related canonical pathways in all diseased PCTS. Most of the culture effects were found in liver, while kidney and ileum PCTS were affected to a lesser extent.

(IIc) Comparative analysis of human diseased vs. healthy PCTS

Genes differentially expressed in diseased and healthy PCTS before and after culture

As a part of the comparative analysis, we investigated the transcripts and pathways differentially regulated in diseased vs. healthy PCTS that were directly affected by pathology and/or culture. Comparison of the baseline transcription profiles (at 0 h) in human PCTS (Fig. 13a; volcano plots in Fig. S10c) showed that healthy and diseased tissues had major differences prior to culturing, as illustrated by a large number of DEGs in liver and kidney PCTS (1500 and 2016 DEGs, respectively). In contrast, only eight genes were differentially expressed at 0 h in diseased ileum PCTS compared to healthy slices. By 48 h of culture, the number of DEGs between diseased and healthy tissues dramatically decreased in all organs, reaching 91% reduction in DEGs in liver, 98% in kidney and 100% in ileum (Fig. 13a; volcano plots in Fig. S10d). Closer examination of these changes showed that in (diseased vs. healthy) liver PCTS, 59% (83 of 141) of DEGs at 48 h were also differentially expressed at 0 h with a consistent direction of regulation (i.e. up- or downregulation). The remaining proportion of regulated transcripts (41%) in diseased vs. healthy liver PCTS was exclusively observed after 48 h culture. In kidney, only 27% (10 of 37) of genes differentially expressed in diseased vs. healthy PCTS at 48 h were also among DEGs at 0 h, while 73% of transcripts were specifically induced by culture. Furthermore, we identified DEGs that showed the strongest differential regulation between healthy and diseased PCTS prepared from the three organs before culture (Fig. 13b) and after 48-h culture (Fig. 13c). The results showed that there were no common top up- and downregulated DEGs between 0 h and 48 h in any organ PCTS. Among the most regulated transcripts, we often encountered genes encoding enzymes, transporters and inflammatory molecules. Additionally, top ten up- and down-regulated DEGs included novel uncharacterized transcripts. The corresponding lists of all DEGs are provided in File S6, and the detailed description of the top ten DEGs are enclosed in Table S6.

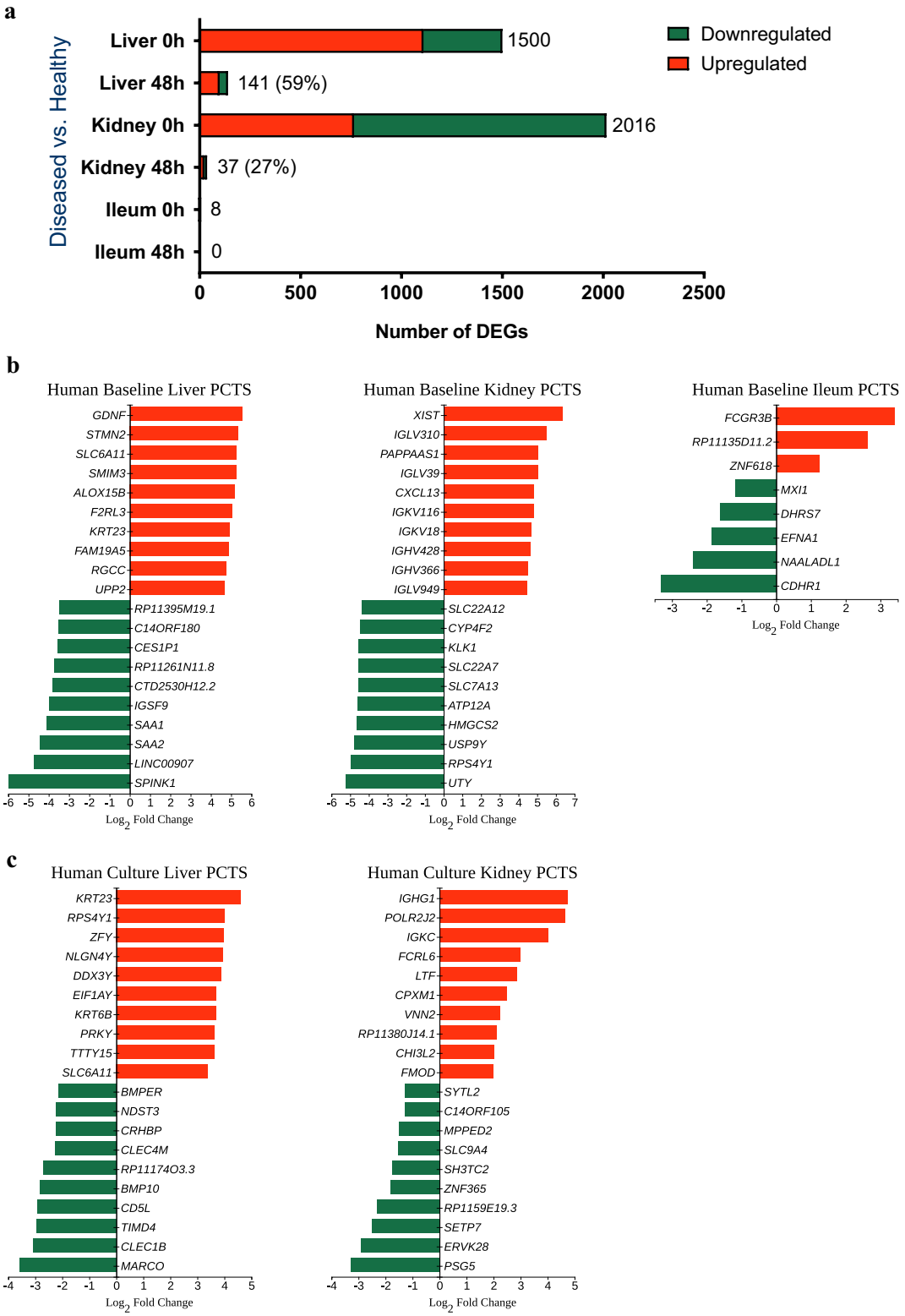

Fig. 13 Comparative analysis of human diseased and healthy PCTS in their baseline expression profiles (0 h) and profiles after 48-h culture. **a** Total number of genes, upregulated and downregulated, that were differentially expressed between diseased and healthy PCTS at 0 h or 48 h. DEGs were defined as genes with $\log_2$ (FC) ≥ 1 and p_{adj} value ≤ 0.01. Numbers in brackets indicate the percentage of DEGs at 48 h that were also DEGs at 0 h. Top ten regulated genes that are differentially expressed between diseased and healthy PCTS at baseline (**b**) and after 48-h culture (**c**). Significantly upregulated DEGs are displayed in red colour and downregulated—in green. Genes were selected based on the $\log_2$ (FC) values. Full lists of identified DEGs are provided in File S7 (colour figure online)

DEGs and enriched canonical pathways in human PCTS induced by pathology

We continued the analysis by elucidating the DEGs and enriched canonical pathways that were induced in human PCTS by pathology. First, we performed pathway analysis on all genes differentially expressed in diseased vs. healthy PCTS prior to culture (as listed in File S6). The results showed that numerous pathology-driven signalling pathways were regulated in liver and kidney PCTS, but not ileum (due to low number of DEGs) (File S7). As an example, before culturing, diseased and healthy liver PCTS showed dramatic difference in regulation of canonical pathway hepatic fibrosis/hepatic stellate cell activation with p value $\leq 10^{-9}$. Next, Venn diagrams illustrated the number of differentially expressed genes in diseased vs. healthy PCTS exclusively before and after culture, as well as numbers of DEGs that were present at both time points (Fig. 14a). Tables with the common and unique genes for each organ can be found in File S8. Each list was ranked by a differential gene expression score (DGE score), which represents the product of $|\log_2(\text{FC})|$ and $-\log_{10}$ (p adjusted value). DEGs unique to diseased vs. healthy PCTS at baseline (0 h) represent the set of transcripts that were induced specifically by pathology. DEGs unique to diseased vs. healthy cultured PCTS (48 h) are the genes that were altered by both pathology and culture. Additionally, the intersection of the two groups represents the common DEGs that were affected by pathology, but not by culture. Next, we performed IPA on DEGs from the Venn diagram intersections to assess the canonical pathways induced by the pathology. In agreement with the small number of common DEGs, there were only five canonical pathways significantly enriched in liver PCTS (Fig. 14b). None of these pathways showed a predicted direction of change. Additionally, we determined signalling pathways that were differentially expressed by diseased and healthy liver and kidney PCTS after 48 h of culture (File S7). The major differences between healthy and diseased PCTS after culture were in pathways related to metabolism.

a

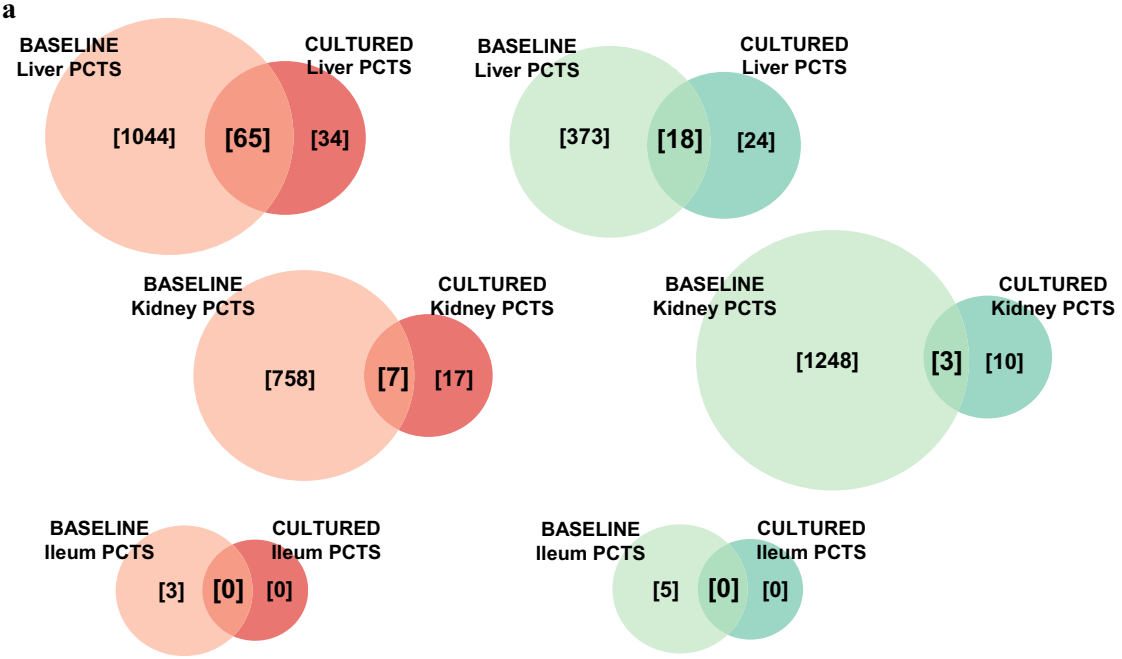

b

		Canonical Pathway	z-score	-log(p-value)	Size	Regulated (%)	Overlap (%)
Enriched from upregulated DEGs	Liver	VDR/RXR Activation	NA	2,88	78	4	18
		GABA Receptor Signaling	NA	2,63	95	3	24
		GP6 Signaling Pathway	NA	2,21	134	2	31
Enriched from downregulated DEGs	Liver	Pregnenolone Biosynthesis	NA	2,11	12	8	58
		Histidine Degradation VI	NA	2,02	15	7	67

Fig. 14 Comparative analysis of baseline expression profiles (0 h) and profiles after 48-h culture in human diseased vs. healthy PCTS. **a** Venn diagrams illustrating the number of unique and overlapping genes upregulated (in red) and downregulated (in green) at 0 h vs. 48 h in human diseased vs. healthy PCTS. Lists of corresponding DEGs can be found in File S9. **b** Top canonical pathways identified by IPA based on common DEGs shown in Venn diagrams. Only liver PCTS had enough common DEGs at baseline vs. 48 h to perform IPA (colour figure online)

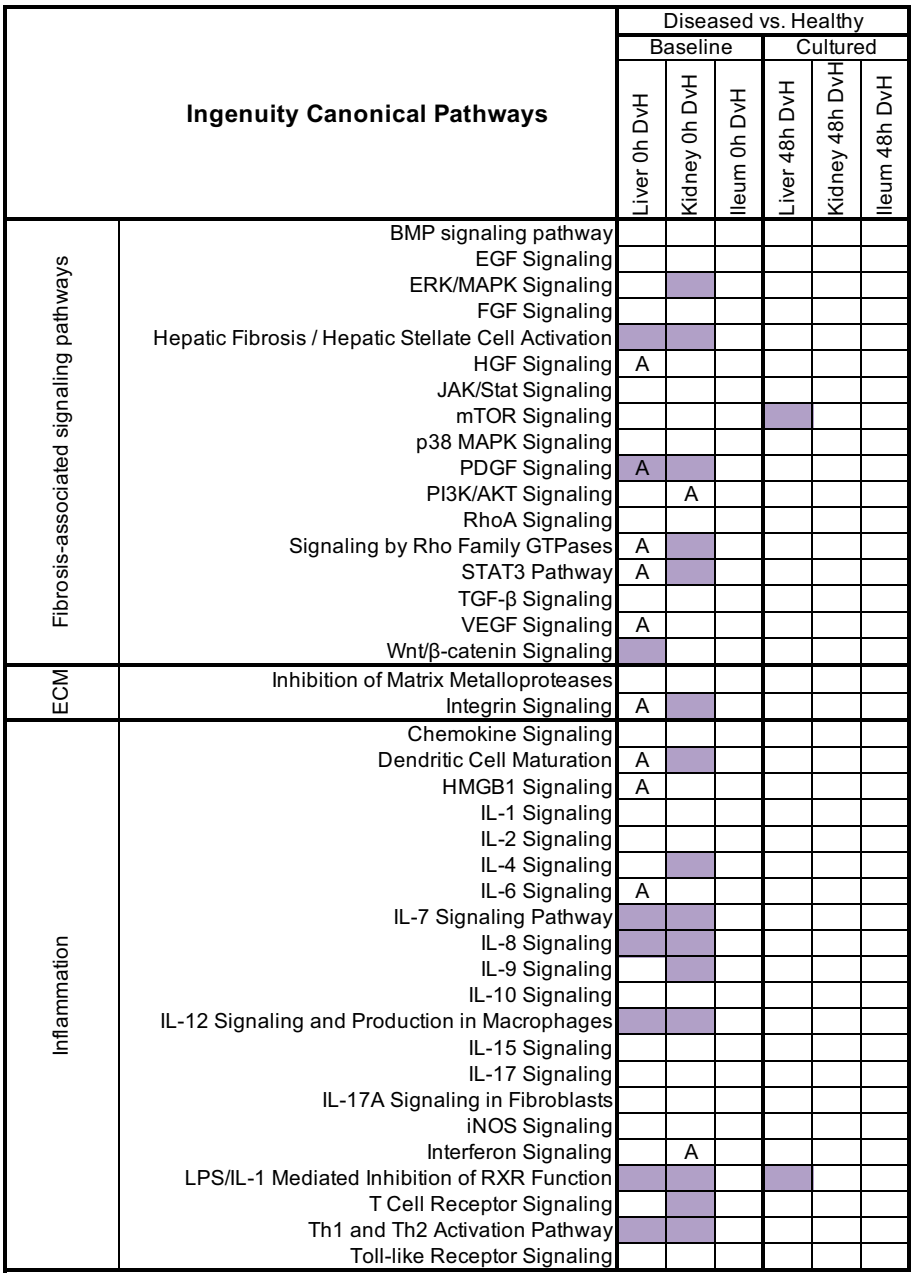

Fig. 15 Differential regulation of preselected pathways between healthy and diseased human PCTS at baseline (0 h) and after 48-h culture. Purple colour indicates a significant pathway change based on a p value ≤ 0.01, whereas predicted pathway activation (A) or inhibition (I) is indicated by a z-score, if available. Signalling molecules involved in each preselected pathway are shown in File S3 (colour figure online)

Differences in regulation of fibrosis- and inflammation-associated pathways in diseased vs. healthy PCTS before and after culture

To advance our understanding of fibrosis and inflammation-associated processes in human PCTS, we investigated differences in the regulation of 40 selected canonical pathways between healthy and diseased PCTS prior and after culture (Fig. 15). In accordance with the reduction in total numbers of DEGs after 48 h, diseased vs. healthy slices showed more differences in regulated canonical pathways at baseline than after culture. In particular, diseased liver PCTS at 0 h showed significant regulation for 16 out of 40 selected pathways (based on both p value and z-score) compared to healthy liver PCTS. In case of kidney PCTS, 17 out of 40 pathways were significantly different due to pathology, and no differences in pathways were observed in ileum PCTS. After 48-h culture, only two pathways were significantly different in diseased liver PCTS compared to healthy slices, whereas no difference in pathway regulation was observed in diseased vs. healthy kidney and ileum PCTS.

a

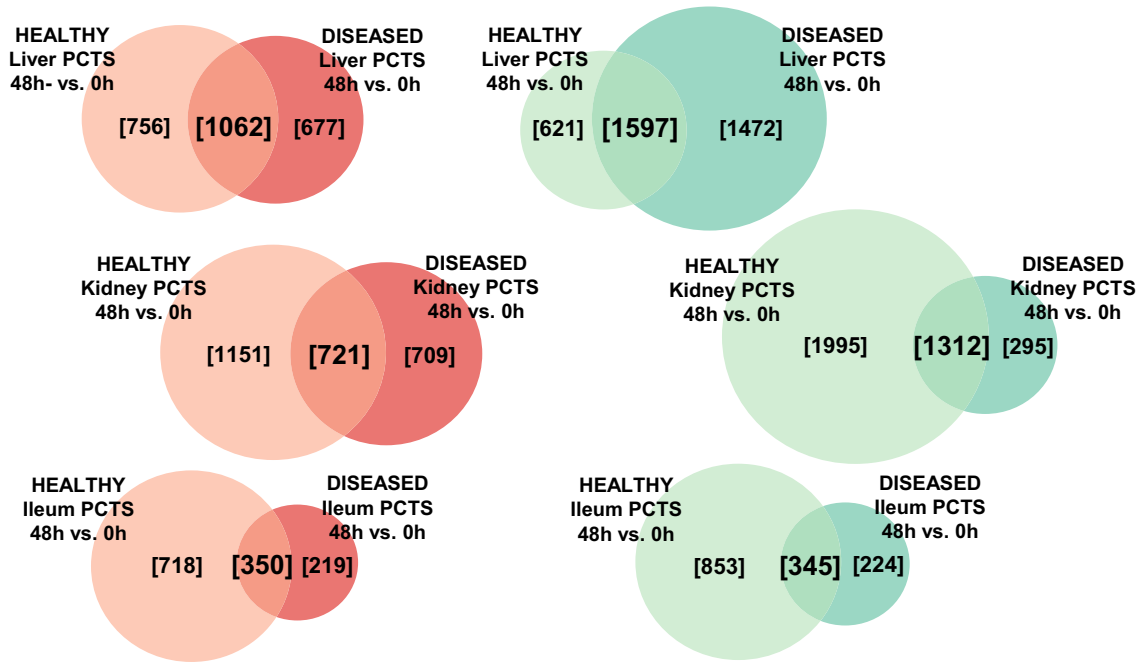

b

		Canonical Pathway	z-score	-log(p-value)	Size	Regulated (%)	Overlap (%)
Enriched from upregulated DEGs	Liver	Integrin Signaling	4,81	7,20	219	13	26
		Signaling by Rho Family GTPases	4,80	4,96	252	11	22
		IL-8 Signaling	4,60	6,79	203	13	28
		Phospholipase C Signaling	4,26	3,89	244	10	22
		Ephrin Receptor Signaling	4,15	8,58	179	16	28
		RhoGDI Signaling	-4,80	8,06	177	15	24
		PTEN Signaling	-2,67	3,55	125	12	21
	Kidney	Osteoarthritis Pathway	3,90	6,85	212	10	27
		IL-8 Signaling	3,77	5,33	203	9	28
		Integrin Signaling	3,64	3,81	219	8	26
		ILK Signaling	3,61	2,87	197	7	24
		Neuroinflammation Signaling Pathway	3,50	2,16	311	5	25
		RhoGDI Signaling	-3,46	2,37	177	7	24
		PPAR Signaling	-2,83	2,13	101	8	21
	Ileum	Osteoarthritis Pathway	3,64	9,07	212	8	27
		IL-8 Signaling	3,61	6,07	203	7	28
		Colorectal Cancer Metastasis Signaling	3,46	3,68	254	5	21
		IL-6 Signaling	3,16	4,79	134	7	24
		Endothelin-1 Signaling	3,00	2,81	196	5	24
		PPAR Signaling	-2,65	3,32	101	7	21
		LXR/RXR Activation	-2,65	4,36	121	7	54
		Antioxidant Action of Vitamin C	-2,45	5,63	108	9	27
Enriched from downregulated DEGs	Liver	LPS/IL-1 Mediated Inhibition of RXR Function	3,67	21,60	222	23	39
		LXR/RXR Activation	-4,74	30,30	121	39	54
		Nicotine Degradation II	-4,47	11,10	65	31	43
		Superpathway of Melatonin Degradation	-4,36	9,49	70	27	39
		Melatonin Degradation I	-4,24	9,18	65	28	37
		cAMP-mediated signaling	-4,15	2,93	228	10	21
	Kidney	Neuroinflammation Signaling Pathway	-4,80	3,41	311	8	25
		Dendritic Cell Maturation	-4,36	3,19	194	10	24
		PKCÎ¸ Signaling in T Lymphocytes	-3,87	3,61	165	11	19
		Role of NFAT in Regulation of the Immune Response	-3,77	3,24	192	10	19
		ILK Signaling	-3,77	2,71	197	9	24
	Ileum	Mitotic Roles of Polo-Like Kinase	-2,45	4,49	66	11	27
		Cyclins and Cell Cycle Regulation	-2,24	3,07	81	7	30
		Estrogen-mediated S-phase Entry	-2,24	4,62	26	19	46

Fig. 16 Comparative analysis of culture-induced changes in expression profiles between healthy and diseased PCTS. **a** Venn diagrams illustrating the number of unique and overlapping genes (DEGs) upregulated (in red) and downregulated (in green) in human healthy and diseased PCTS during 48-h culture. Total numbers of culture-induced DEGs in PCTS from diseased liver, kidney and ileum are illustrated in Fig. 11a, while total numbers of DEGs found in healthy PCTS are depicted in Fig. 3b in Part I. Complete lists of DEGs are provided in File S6. **b** Top canonical pathways enriched from common culture-induced DEGs present in both healthy and diseased PCTS. Only pathways with p value ≤ 0.01 and a z-score ≥ 2 (predictor of activation) or ≤ -2 (predictor of inhibition) were included. Pathway size (i.e. total number of genes in a pathway), percentage of significantly downregulated (green bars) and upregulated (red bars) genes in a given pathway, and percentage of overlap with the dataset (grey bars) are indicated for each pathway (colour figure online)

DEGs and enriched canonical pathways induced in healthy and diseased PCTS during culture

Considering that healthy (Part I) and diseased PCTS developed substantial transcriptional alterations during 48 h culture, we determined genes and canonical pathways that are culture affected in both healthy and diseased tissues. First, we identified common and unique culture-induced DEGs (up- and down-regulated) in healthy and diseased PCTS (Fig. 16a). To this end, we compared all DEGs found in diseased PCTS (Fig. 16a) to all DEGs reported in healthy PCTS (Part I, Fig. 3b). Unique DEGs were affected by culture and pathology (i.e. expressed only in healthy or diseased PCTS), whereas DEGs in intersections were transcripts affected by culture. The complete lists of all DEGs included in Venn diagrams are shown in File S9. As a next step of the analysis, we performed IPA on overlapping gene sets. The most significant canonical pathways enriched from these gene sets are summarized in Fig. 16b. Culture-induced pathways across healthy and diseased PCTS included activated pathways, such as osteoarthritis pathway, IL-8 signalling and integrin signalling, and inhibited pathways, such as LXR/RXR activation, PPAR signalling and RhoGDI signalling. Of note, canonical pathways enriched from downregulated DEGs were more organ specific, and were related to metabolism, inflammation and cell cycle regulation.

Cytokine release profiles of human healthy and diseased PCTS

As part of cellular mechanisms of fibrosis, damaged epithelial cells and (resident) immune cells secrete various cytokines that drive the inflammatory and fibrogenic responses (Wynn 2004). Along with the transcriptional changes, we assessed PCTS cytokine release profiles during 48 h to examine whether diseased and healthy PCTS display differences in production of inflammatory mediators. To this end, we analysed the culture medium for the presence of 42 cytokines and cytokine modulators (all measurements are included in File S10). We selected 29 cytokines for further analysis based on two criteria: (1) minimum concentration of 20 pg/mL detected in the medium in at least one experimental condition, and (2) significant regulation on gene expression level. The independent hierarchical clustering separated diseased liver and kidney PCTS from the corresponding healthy slices, suggesting considerable pathology-driven differences in cytokine release (Fig. 17a). In turn, diseased and healthy ileum PCTS had very close resemblance in their cytokine release profiles, which distinguished them from the other two organs. PCTS displayed few characteristic features in cytokine release. For instance, healthy liver PCTS showed higher production of IL-7 and SAA1, compared to diseased liver and other organ PCTS. In turn, diseased liver PCTS produced more IL-16 and HGF than healthy slices. Healthy and diseased kidney PCTS released more MCP-1 and OPN compared to other slices. Furthermore, diseased kidney showed the highest release of most tested analytes among all human PCTS. Lastly, healthy and diseased ileum highly secreted IL-12A, IL-17A, MMP2, MMP3, IFNG and GM-SCF.

Next, to address the question whether gene expression of selected cytokines reflected their protein levels, we performed correlation analysis (Fig. 17b). In general, in all organ PCTS, high gene expression of inflammatory mediators was positively associated (approximately 45–70%) with high level of their protein release. Interestingly, all human healthy and diseased PCTS showed both high expression and secretion of TIMP1, a cytokine with enzymatic activity that inhibits ECM degradation by MMPs. Additionally, all kidney PCTS and diseased liver slices showed high gene and protein expression of MCP-1 (encoded by *CCL2*) and OPN (encoded by *SPP1*) during culture, when taking into account both MSD and RNA-Seq results. Both MCP-1 (monocyte chemoattractant protein 1) and OPN (osteopontin) are actively involved in the inflammatory response and fibrogenesis by promoting the recruitment of immune cells to the site of tissue injury. Organ differences in cytokine regulation are also highlighted by the correlation study, as liver PCTS highly expressed and secreted SAA1, while MMP2 and MMP3 were characteristic for ileum PCTS. SAA1, serum amyloid A1, is a major acute-phase response protein that is predominantly secreted by hepatocytes. Similar to MCP-1 and OPN, SAA1 induces chemotaxis in inflammatory cells and their cytokine/chemokine production (Sack 2018). This pro-inflammatory mediator has also been shown to upregulate ECM-degrading enzymes (MMPs) (Sack 2018). Taken together, these results showed that pre-existing pathology accentuates cytokine production in human PCTS, with positive association between protein and mRNA levels, especially for cytokines with relatively high levels of gene expression and gene protein product release.

Discussion

Among different in vitro/ex vivo preparations of human organs, precision-cut tissue slices (PCTS) represent a system with particularly high similarity to the originating organ. Among the wide range of applications, the PCTS model is gaining its value in studying the mechanisms of organ fibrosis and antifibrotic compounds. However, the molecular processes that occur in PCTS during culture remain largely uncharacterized, preventing the adoption of PCTS model in preclinical research to its full potential. In this study, we sequenced total RNA of PCTS prepared from human healthy and diseased liver, kidney and ileum

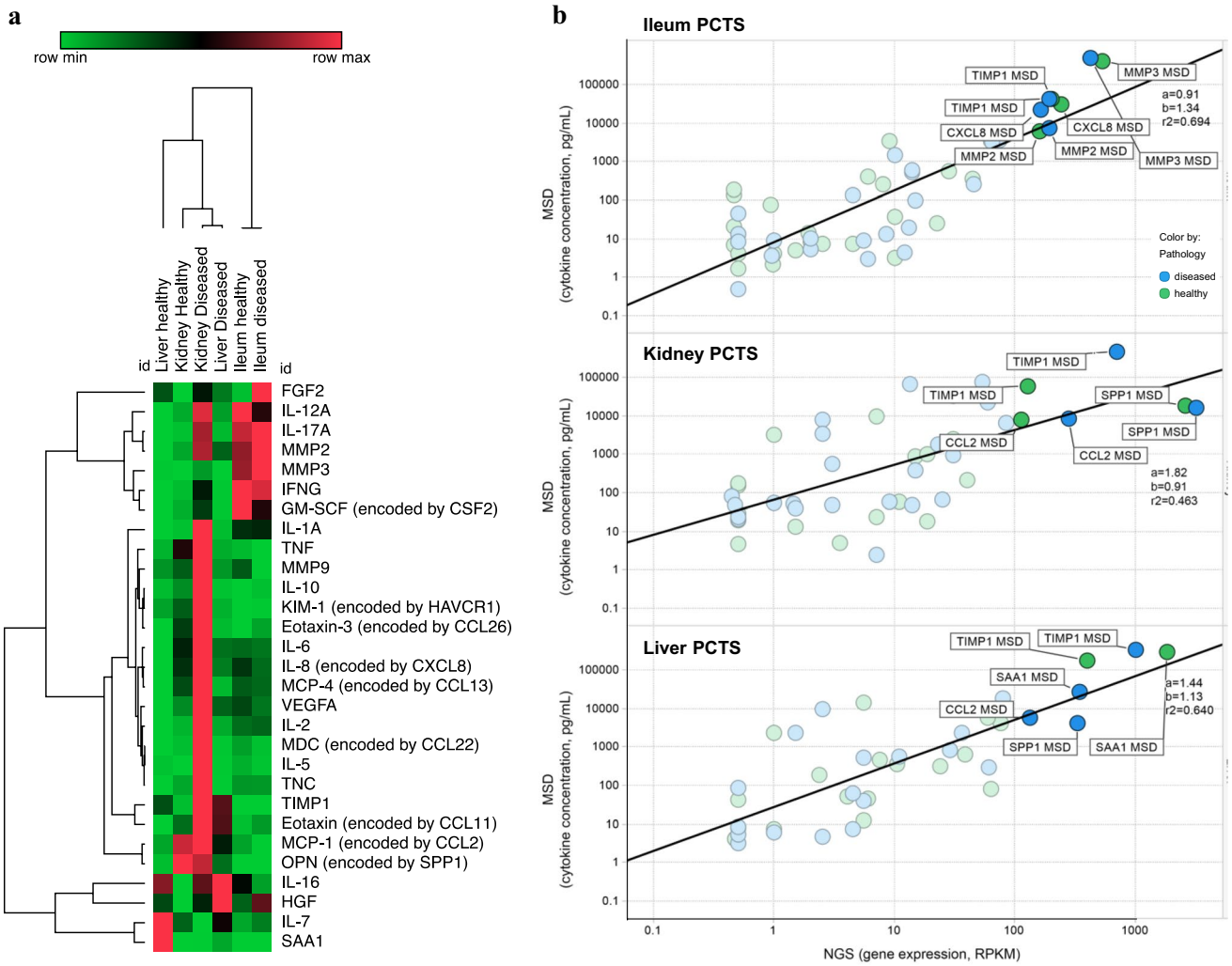

Fig. 17 Cytokine release by human healthy and diseased PCTS after 48 h in culture. **a** Heatmap of the absolute concentrations (pg/mL) illustrates cytokine release profile of human healthy and diseased PCTS. PCTS from liver, kidney and ileum were incubated for 48 h, culture medium was collected after 24 h and 48 h and tested for the presence of selected cytokines using Meso Scale Discovery (MSD) multiplex assay. For each cytokine, concentrations measured at 24 h and 48 h were normalized to the negative control (i.e. freshly prepared medium) and summed to determine total cytokine concentration at the end of culture period. **b** Correlation analysis of the relationship between cytokine protein expression (as measured by MSD) and gene expression (as measured by NGS/RNA-Seq). Each dot represents one cytokine; green colour codes healthy PCTS, while blue colour codes diseased PCTS. Highly expressed cytokines (i.e. > 100 RPKM on gene level and > 1000 pg/mL on protein level) are annotated

with the aim to elucidate culture-driven transcriptional changes, especially those related to inflammation and fibrosis. We characterized diseased PCTS in culture by describing main differentially expressed transcripts and culture-affected biological pathways. Furthermore, we demonstrated that culture impacts healthy and diseased tissue slices in a universal way, converging them to a common, inflammation- and fibrosis-driven condition with limited transcriptional differences between healthy and diseased PCTS, while the underlying pathology endures.

Culture impacts human PCTS from healthy and diseased tissues in a universal way, triggering mechanisms of wound healing and fibrosis

Preparation of the tissue slices causes significant injury as a result of a combination of cold ischemia prior to slicing and mechanical trauma during slicing, both of which are inevitable. It has to be noted that all human tissues—clinically healthy and diseased—were obtained from patients that suffered from cancer or fibrotic diseases, other injury

or bleeding and underwent surgical procedure. These might influence the initial transcriptional background of human tissues, including healthy control samples, since it was shown that surgical intervention causes an acute-phase response and increase in cytokine production (de Jong et al. 2004).

It is well recognized that in response to the injury, various organs share common mechanisms associated with wound healing and fibrosis (Zeisberg and Kalluri 2013; Rockey et al. 2015). Culturing of the slices prompts the progression of fibrosis by driving an environment of sustained injury. Indeed, human PCTS of different organ of origin and pre-existing pathology showed similarities in the way that culture affected their transcriptional profiles, supporting that culture triggers common mechanisms of wound healing and fibrosis.

Our Part I study showed that human PCTS prepared from healthy tissues undergo substantial transcriptional changes during culture, with thousands of differentially expressed genes. Here we show that culture also induced pronounced transcriptional changes in PCTS from diseased tissues, counted in thousands of genes as well, pushing the diseased slices beyond their initial pathology. The comparison of these changes in healthy and diseased PCTS (Fig. 10: DEGs A–A' vs. DEGs B–B') delineated universal impact of culture on human tissues. We demonstrated that all human PCTS, regardless the originating organ or pre-existing pathology, displayed, on one hand, culture-induced inflammatory response and matrix remodelling, and on the other hand, dysregulated enzymatic and transporter activity, as illustrated by identified common transcripts and biological pathways.

For instance, transcripts encoding inflammatory cytokine IL-11 and ECM-degrading enzymes MMP1, MMP3 and MMP10 were found among the DEGs with the highest fold change in all diseased PCTS (Fig. 11b)—the same transcripts that were strongly upregulated across healthy human PCTS, as reported in Part I of this study. The homogeneity in the effects of culture is further illustrated by the fact that diseased liver, kidney and ileum PCTS shared five out of ten top upregulated genes during culture with the respective healthy slices, while the majority of other 5 genes was also shared but outside the top 10 list (instead, these were shared within top 100). As an example, SERPINB2, encoding plasminogen activator inhibitor type 2 (PAI-2), was identified as the gene with the highest fold change among all DEGs in healthy and diseased kidney PCTS (i.e. ranked first in the top ten upregulated genes), and it was also significantly upregulated during culture in other organ PCTS, only with a smaller fold change. PAI-2 is a stress protein expressed in activated monocytes and macrophages and is highly inducible in fibroblasts and endothelial cells (Kruithof et al. 1995; Medcalf and Stasinopoulos 2005). PAI-2 transcription is stimulated by a variety of inflammatory mediators, suggesting its biological role in the regulation of inflammation and wound healing (Medcalf and Stasinopoulos 2005). Additionally, most of the common DEGs with the highest differential gene expression score (DGE score), affected by culture in both healthy and diseased PCTS, were also related to ECM organisation (Fig. 13a, File S7), supporting the idea that culture augments fibrosis-associated tissue remodelling in healthy and diseased slices alike. As an example, healthy and diseased liver PCTS showed significant upregulation after the culture of *NID2*, *LAMA4* and *ITGA2* that encode the ECM structural constituents nidogen, laminin and integrin, respectively. Additionally, healthy and diseased liver PCTS highly expressed latexin (encoded by *LXN*), which serves as a marker of portal myofibroblasts (Lemoinne et al. 2013), and epoxide hydrolase 4 (encoded by *EPHX4*), which reduces bioactivity of fatty acids (Lord et al. 2013). The latter is in accordance with the observed inhibition of LXR/RXR activation and fatty acid beta-oxidation pathways. Similarly, culture enhanced upregulation of *ZPLD1*, *ITGB3* and *ITGB6* in healthy and diseased kidney slices. While *ITGB3* and *ITGB6* encode integrins that bind to ECM proteins, *ZPLD* encodes ECM glycoprotein zona pellucida-like domain-containing 1 although little is known about its function (Hynes and Naba 2012). Furthermore, as found previously, both healthy and diseased ileum PCTS highly express ECM-related genes *MMP1* and *MMP3*. Culturing of the slices was also associated with altered enzymatic and transporter activity, as top downregulated genes in healthy and diseased PCTS encoded various enzymes and transporters although these had more diversity between the organs (Figs. 11b and 4b in Part I).

The commonalities in culture-induced transcripts translated into commonly regulated biological pathways in healthy and diseased PCTS. Cross-comparison of identified culture-induced biological pathways in diseased PCTS (Fig. 11c) with the data on human healthy PCTS reported in Part I, revealed that diseased liver, kidney and ileum PCTS shared 90%, 35% and 60% of activated by culture pathways with corresponding healthy organ slices, respectively. In turn, 60%, 60% and 20% of inhibited pathways were the same between healthy and diseased liver, kidney and ileum PCTS, respectively. The homogeneity of culture effects on tissue slices was further supported by the fact that all human PCTS, regardless of the originating organ or pre-existing pathology, showed consistent significant activation of osteoarthritis pathway and inhibition of LXR/RXR activation during culture. The implications of the latter were discussed in detail in Part I; therefore, here we will address the former. As a fibrosis-associated disease, osteoarthritis is characterized by extensive structural changes in ECM under inflammatory conditions that ultimately leads to joint stiffness and disability (Hill et al. 2007; Remst et al. 2015). According to IPA, osteoarthritis pathway involves over 200 transcripts,

encoding ECM structural components (e.g. collagens, integrins, fibronectin and decorin), ECM remodelling enzymes (MMPs and TIMPs), inflammatory molecules (e.g. IL-1B, CXCL8, TNF, TLR2 and TLR4, to name a few), as well as downstream molecules of TGF, PDGF, VEGF, FGF, WNT and SHH signalling cascades, among others. The fact that osteoarthritis pathway is significantly activated in all human PCTS at 48 h and in murine PCTS (as found in Part I) suggests that culture sustains pro-inflammatory and profibrotic environment.

Among other shared canonical pathways, actin nucleation by ARP–WASP complex and ephrin receptor signalling were activated by culture in liver and kidney PCTS, both healthy and diseased. Actin nucleation by ARP–WASP complex is known to promote cell migration (Kaverina et al. 2003; Yamaguchi et al. 2005), a phenomenon that plays an important role in tissue fibrosis, as migration of fibroblasts toward fibrotic lesions is essential for pathological matrix deposition (Tschumperlin 2013). In turn, the Eph receptors and their ligands ephrins play an important role in injury (in particular, wound healing and ischemia–reperfusion injury) and inflammation (Coulthard et al. 2012). It has been shown that Eph receptor EPHB2 is overexpressed in hepatocellular carcinoma, end stage of liver fibrosis/cirrhosis and in other fibrotic diseases (Hafner 2004; Mimche et al. 2018). At last, we demonstrated that common DEGs after 48-h culture between healthy and diseased PCTS additionally enriched IL-8 signalling and integrin signalling (Fig. 11b), supporting our observation that culture induces inflammation- and fibrosis-associated biological processes in tissue slices. Interestingly, part of the analysis that was dedicated to the regulation of selected pathways in diseased PCTS showed that even though culture augmented transcriptional changes in inflammatory and fibrosis pathways in all organ PCTS, diseased liver PCTS displayed the most pronounced changes (Fig. 12). Taken together, these observations reinforce the use of human PCTS as an ex vivo fibrosis model.

Organ- and pathology-specificity in the effect of culture

Despite the described uniformity in the effects of culture on tissue slices, our comprehensive sequencing data allowed to detect organ-specific differences in transcriptional changes between liver, kidney and ileum PCTS. We chose to exemplify such differences with intestinal PCTS although similar critical examination can be done for liver and kidney PCTS.

On the gene expression level, we identified several transcripts—*DUOX2, DUOXA2, CEMIP* and *CHI3L1*—that were strongly upregulated during culture only in human intestinal PCTS, regardless of the pre-existing pathology. Dual oxidase 2, encoded by *DUOX2*, is an intestinal epithelium-specific NADPH oxidase that plays a critical role in the innate defense response against the microbiota by generating reactive oxygen species (El Hassani et al. 2005; Grasberger et al. 2015). It has been shown that both DUOX2 and its maturation factor DUOXA2 are upregulated in association with chronic inflammatory disorders of the gastrointestinal tract, such as Crohn's disease (CD), ulcerative colitis (UC) and UC-associated colorectal cancer (MacFie et al. 2014; Haberman et al. 2014). In turn, expression of endosomal cell migration-inducing and hyaluronan-binding protein (CEMIP) is highly elevated in colorectal cancer although its role remains unclear (Fink et al. 2015). Gene *CHI3L1* encodes chitinase-3-like protein 1 (also known as BRP-39), a marker for late stages of macrophage differentiation (Rehli et al. 2003). Dysregulation of BRP-39 is often associated with human diseases characterized by acute or chronic inflammation and fibrosis (Lee et al. 2011).

Similarly, organ-specific differences can be traced on the pathway level. For instance, both healthy and diseased ileum PCTS displayed (almost exclusively) significant activation of colorectal cancer metastasis signalling and IL-6 signalling. Closer examination of the activated biological pathways also suggests pathology-specific differences in the effects of culture on human PCTS. We found that PCTS from healthy tissues seem to develop stronger inflammatory response during culture than diseased PCTS, as they shared more activated inflammation-related pathways. That could be due to the fact that diseased tissues, unlike healthy tissues, have already passed the initial inflammatory phase and are at the stage of fibrosis progression. Another example of pathology-specific differences is the culture-induced activation of p53 signalling in diseased liver PCTS and not in healthy slices. It is well established that tumor suppressor p53 is highly sensitive to DNA damage and cellular stress and regulates cell fate by directing damaged cells down the cell cycle arrest or apoptosis (Kastenhuber and Lowe 2017). Therefore, p53 signalling plays a central role in tumorigenesis and prognosis of hepatocellular carcinoma (Kunst et al. 2016). Considering that PCTS were prepared from cirrhotic livers that had considerable pre-existing DNA and cellular damage, culture induced activation of p53 pathway in these slices. In turn, diseased kidney and ileum PCTS actively involved pathways related to cholesterol biosynthesis, as opposed to healthy PCTS. We should note that cholesterol biosynthesis mainly takes place in the liver, but there were no significant changes in its regulation during culture in healthy or diseased liver PCTS.

Culturing process drives a common fibrosis-associated state for healthy and diseased PCTS, while preserving diseased PCTS phenotype

Directly after slicing, healthy and diseased PCTS displayed pronounced differences in their transcriptomes that were driven solely by pre-existing pathology (Fig. 10: DEGs

A–B). Similar to this observation, we previously demonstrated clear diseased phenotype of PCTS prepared from fibrotic kidneys: compared to healthy slices, fibrotic kidney PCTS showed significantly higher baseline levels of *COL1A1, FN1, IL1B, IL6, CXCL8* and *TNF*, as well as increased accumulation of interstitial collagen type I and alpha-SMA (unpublished data).

The obtained sequencing data allowed to identify the top pathology-driven transcripts differentially regulated between healthy and diseased PCTS. Here we took kidney PCTS as an example; however, an in-depth examination of transcriptional differences prior to culture in kidney and other organ PCTS is not a focus of this discussion. Among 2016 genes differentially expressed between healthy and diseased kidney PCTS (Fig. 14a), we found that 47 transcripts, encoding immunoglobulins (IGs), were highly upregulated in diseased kidney PCTS (with the highest fold increase of 45) (Fig. 14b and File S9). IGs are a critical part of the immune response, and increased mRNA levels of IGs might indicate active/chronic inflammatory processes in diseased kidney PCTS. Highly upregulated CXCL13 (with 28-fold increase) further argues for the uncontrolled aberrant inflammation in diseased renal tissue (Sato and Yanagita 2017). Gene *UTS2*, with 19-fold increase in diseased kidney PCTS compared to healthy PCTS, encodes urotensin II that has been shown to promote fibrosis, and its upregulated levels were observed in patients in the later stages of chronic kidney disease (CKD), particularly in individuals requiring dialysis (Eyre et al. 2019).

While liver and kidney PCTS showed pathology-driven differential expression of thousands of genes, healthy and diseased ileum PCTS failed to show differences in baseline transcriptomes. This could be associated with the way human intestinal slices are prepared. Prior to slicing, the mucosa is stripped from all other layers, including submucosa, muscularis externa and serosa, due to the technical difficulties they impose. In case of diseased ileum PCTS, the removal of deeper intestinal layers was detrimental to manifest their diseased phenotype. Intestinal fibrosis often follows the distribution of inflammation and is not necessarily restricted to mucosa: in UC, the deposition of ECM occurs in mucosal and submucosal layers, whereas in CD, fibrosis can involve all intestinal wall layers (Rieder et al. 2007; Speca 2012). Therefore, preparation of human intestinal PCTS should be further optimized.

Remarkably, as both healthy and diseased PCTS demonstrated extensive transcriptional changes during culture, after 48 h they showed minimal differences in acquired transcriptomes (counted in only tens/hundreds of DEGs) (Fig. 10: DEGs A'–B'). These observations indicate that during ex vivo culture, healthy and diseased human PCTS converge to a common condition, which is largely prompted by inflammatory and fibrogenic processes. This study provides a transcriptomic baseline for PCTS culture; how this resulting condition is predictive for human pathological processes is yet to be determined. Furthermore, the signature of pre-existing pathology remains in cultured slices and it may affect biological events other than gene regulation. For instance, underlying pathology may influence cell–cell interactions, production of ECM proteins, growth factors and cytokines. As we demonstrated, diseased PCTS had an increased production of cytokines and cytokine modulators compared to healthy PCTS, emphasizing the value of diseased human tissue in fibrosis studies using the PCTS model. Importantly, the production of cytokines reflected the changes in their gene expression in PCTS during culture. Although protein synthesis and release are influenced by many cellular and molecular regulatory processes, the observed positive correlation between protein release and gene expression data argues for the fact that transcriptional changes detected by NGS are to some extent predictive for translational changes. However, it is important to continue investigating whether observed transcriptional changes in PCTS indeed translate to the protein level, by systematic analysis of the proteome. Given these points, PCTS obtained from patient diseased tissues might provide relevant insights into fibrosis, therapeutic target validation and drug development.

Conclusions

In this study, we employed whole transcriptome sequencing to uncover the molecular processes that characterize PCTS culture. In Part I, we investigated species and organ differences in culture-associated responses in healthy murine and human PCTS. Part II of this study delineates the molecular processes in cultured human PCTS generated from diseased (fibrotic) tissues. Furthermore, we performed comparative analysis of transcriptomic profiles of human diseased and healthy control PCTS. In conclusion,

- We provided extensive characterization of the dynamic transcriptional changes in murine and human PCTS during culture.
- We demonstrated that culture impacts all PCTS in a universal way by actively inducing inflammatory response and fibrosis-associated ECM remodelling. Despite the converging effects of culture, the underlying pathology in human diseased PCTS endures and influences biological processes such as cytokine release. This emphasizes the importance of using both healthy and diseased tissues in basic research and drug development.
- Although many pathways were shared, PCTS of different species and organs displayed an individualized response during culture.

- Investigation of molecular processes that are similar in murine and human PCTS contributes to the understanding of how mice fit into drug development of therapeutics for human diseases. However, how well the PCTS model reflects the in vivo situation is yet to be determined.

Taken together, our study largely contributes to our understanding of molecular mechanisms involved in PCTS culture and reinforces their use as an ex vivo fibrosis model, that is suitable for functional investigation of antifibrotic and anti-inflammatory therapies. This lays the foundation for future studies towards the assessment of predictivity of PCTS for human diseases and their validation as a preclinical tool for drug development.

Acknowledgements The authors thank the abdominal transplantation surgeons of the Department of Hepato-Pancreato-Biliary Surgery and Liver Transplantation and surgeons of the Department of Urology (especially I.J. de Jong and A.M. Leliveld), University Medical Center Groningen for providing human tissue. We also would like to thank Dr. Tobias Hildebrandt and Werner Rust from the BI Genomics Lab for carrying out the RNA extraction and Next-Generation Sequencing of the PCTS. This work was kindly supported by ZonMW (The Netherlands Organization for Health Research and Development), Grant no. 114025003.

Author contributions EB, EG, JFR and PO designed the study. PO acquired funding for this study. EB and EG prepared and collected mouse and human samples. KPdJ and HSH helped with human tissue procurement. ES and MZ carried out the sequencing and data analysis. EB, EG and MB interpreted the data. EB and EG wrote the manuscript with critical review from ES, MZ, AO, KPdJ, MS, PN, JFR and PO.

Compliance with ethical standards

Conflict of interest Eric Simon, Matthias Zwick, Anouk Oldenburger, Marco Schlepütz, Paul Nicklin and Jörg F. Rippmann are full employees of Boehringer Ingelheim Pharma GmbH & Co. KG.

References

Alsafadi HN, Staab-Weijnitz CA, Lehmann M et al (2017) An ex vivo model to induce early fibrosis-like changes in human precision-cut lung slices. Am J Physiol Cell Mol Physiol 312:L896–L902. https://doi.org/10.1152/ajplung.00084.2017

Barksby HE, Milner JM, Patterson AM et al (2006) Matrix metalloproteinase 10 promotion of collagenolysis via procollagenase activation: implications for cartilage degradation in arthritis. Arthritis Rheum 54:3244–3253. https://doi.org/10.1002/art.22167

Bar-Or D, Rael LT, Thomas GW, Brody EN (2015) Inflammatory pathways in knee osteoarthritis: potential targets for treatment. Curr Rheumatol Rev 11:50–58. https://doi.org/10.2174/1573397111666150522094131

Bhattacharyya S, Midwood KS, Yin H, Varga J (2017) Toll-like receptor-4 signaling drives persistent fibroblast activation and prevents fibrosis resolution in scleroderma. Adv Wound Care 6:356–369. https://doi.org/10.1089/wound.2017.0732

Bigaeva E, Bomers JJM, Biel C et al (2019) Growth factors of stem cell niche extend the life-span of precision-cut intestinal slices in culture: a proof-of-concept study. Toxicol Vitro 59:312–321. https://doi.org/10.1016/j.tiv.2019.05.024

Boztepe T, Gulec S (2018) Investigation of the influence of high glucose on molecular and genetic responses: an in vitro study using a human intestine model. Genes Nutr 13:11. https://doi.org/10.1186/s12263-018-0602-x

Bull DA, Reid BB, Connors RC et al (2000) Improved biochemical preservation of heart slices during cold storage. Int J Surg Investig 2:117–123

Chakraborty D, Šumová B, Mallano T et al (2017) Activation of STAT3 integrates common profibrotic pathways to promote fibroblast activation and tissue fibrosis. Nat Commun 8:1130. https://doi.org/10.1038/s41467-017-01236-6

Cheng R, Takahashi Y, Shen W et al (2013) Pathogenic role of diabetes-induced PPAR- down-regulation in microvascular dysfunction. Proc Natl Acad Sci 110:15401–15406. https://doi.org/10.1073/pnas.1307211110

Coulthard MG, Morgan M, Woodruff TM et al (2012) Eph/Ephrin signaling in injury and inflammation. Am J Pathol 181:1493–1503. https://doi.org/10.1016/j.ajpath.2012.06.043

de Graaf IA, Groothuis GM, Olinga P (2007) Precision-cut tissue slices as a tool to predict metabolism of novel drugs. Expert Opin Drug Metab Toxicol 3:879–898. https://doi.org/10.1517/17425255.3.6.879

de Graaf IAM, Olinga P, de Jager MH et al (2010) Preparation and incubation of precision-cut liver and intestinal slices for application in drug metabolism and toxicity studies. Nat Protoc 5:1540–1551. https://doi.org/10.1038/nprot.2010.111

de Jong KP, Hoedemakers RMJ, Fidler V et al (2004) Portal and systemic serum growth factor and acute-phase response after laparotomy or partial hepatectomy in patients with colorectal liver metastases: a prognostic role for C-reactive protein and hepatocyte growth factor. Scand J Gastroenterol 39:1141–1148. https://doi.org/10.1080/00365520410009609

de Kanter R, Tuin A, van de Kerkhof E et al (2005) A new technique for preparing precision-cut slices from small intestine and colon for drug biotransformation studies. J Pharmacol Toxicol Methods 51:65–72. https://doi.org/10.1016/j.vascn.2004.07.007

Dimitriadis G, Mitrou P, Lambadiari V et al (2011) Insulin effects in muscle and adipose tissue. Diabetes Res Clin Pract 93:S52–S59. https://doi.org/10.1016/S0168-8227(11)70014-6

Domínguez-Avila J, González-Aguilar G, Alvarez-Parrilla E, de la Rosa L (2016) Modulation of PPAR expression and activity in response to polyphenolic compounds in high fat diets. Int J Mol Sci 17:1002. https://doi.org/10.3390/ijms17071002

El Hassani RA, Benfares N, Caillou B et al (2005) Dual oxidase2 is expressed all along the digestive tract. Am J Physiol Liver Physiol 288:G933–G942. https://doi.org/10.1152/ajpgi.00198.2004

Elferink MGL, Olinga P, van Leeuwen EM et al (2011) Gene expression analysis of precision-cut human liver slices indicates stable expression of ADME-Tox related genes. Toxicol Appl Pharmacol 253:57–69. https://doi.org/10.1016/J.TAAP.2011.03.010

Eyre HJ, Speight T, Glazier JD et al (2019) Urotensin II in the development and progression of chronic kidney disease following 5/6 nephrectomy in the rat. Exp Physiol 104:421–433. https://doi.org/10.1113/EP087366

Fink SP, Myeroff LL, Kariv R et al (2015) Induction of KIAA1199/CEMIP is associated with colon cancer phenotype and poor

patient survival. Oncotarget 6:30500–30515. https://doi.org/10.18632/oncotarget.5921
Fromenty B, Pessayre D (1995) Inhibition of mitochondrial beta-oxidation as a mechanism of hepatotoxicity. Pharmacol Ther 67:101–154. https://doi.org/10.1016/0163-7258(95)00012-6
Geurts N, Martens E, Van Aelst I et al (2008) β-hematin interaction with the hemopexin domain of gelatinase B/MMP-9 provokes autocatalytic processing of the propeptide, thereby priming activation by MMP-3†. Biochemistry 47:2689–2699. https://doi.org/10.1021/bi702260q
Gierut A, Perlman H, Pope RM (2010) Innate immunity and rheumatoid arthritis. Rheum Dis Clin North Am 36:271–296. https://doi.org/10.1016/j.rdc.2010.03.004
Grasberger H, Gao J, Nagao-Kitamoto H et al (2015) Increased expression of DUOX2 is an epithelial response to mucosal dysbiosis required for immune homeostasis in mouse intestine. Gastroenterology 149:1849–1859. https://doi.org/10.1053/j.gastro.2015.07.062
Haberman Y, Tickle TL, Dexheimer PJ et al (2014) Pediatric Crohn disease patients exhibit specific ileal transcriptome and microbiome signature. J Clin Invest 124:3617–3633. https://doi.org/10.1172/JCI75436
Hafner C (2004) Differential gene expression of EPH receptors and ephrins in benign human tissues and cancers. Clin Chem 50:490–499. https://doi.org/10.1373/clinchem.2003.026849
Heberle H, Meirelles GV, da Silva FR et al (2015) InteractiVenn: a web-based tool for the analysis of sets through Venn diagrams. BMC Bioinform 16:169. https://doi.org/10.1186/s12859-015-0611-3
Heimburger M, Larfars G, Bratt J (2000) Prednisolone inhibits cytokine-induced adhesive and cytotoxic interactions between endothelial cells and neutrophils in vitro. Clin Exp Immunol 119:441–448. https://doi.org/10.1046/j.1365-2249.2000.01165.x
Hill CL, Hunter DJ, Niu J et al (2007) Synovitis detected on magnetic resonance imaging and its relation to pain and cartilage loss in knee osteoarthritis. Ann Rheum Dis 66:1599–1603. https://doi.org/10.1136/ard.2006.067470
Ho JK, Duclos RI, Hamilton JA (2002) Interactions of acyl carnitines with model membranes. J Lipid Res 43:1429–1439. https://doi.org/10.1194/jlr.M200137-JLR200
Hynes RO, Naba A (2012) Overview of the matrisome—an inventory of extracellular matrix constituents and functions. Cold Spring Harb Perspect Biol 4:a004903. https://doi.org/10.1101/cshperspect.a004903
Iswandana R, Pham BT, van Haaften WT et al (2016) Organ- and species-specific biological activity of rosmarinic acid. Toxicol Vitr 32:261–268. https://doi.org/10.1016/j.tiv.2016.01.009
Kasper M, Seidel D, Knels L et al (2004) Early signs of lung fibrosis after in vitro treatment of rat lung slices with CdCl2 and TGF-β1. Histochem Cell Biol 121:131–140. https://doi.org/10.1007/s00418-003-0612-6
Kastenhuber ER, Lowe SW (2017) Putting p53 in context. Cell 170:1062–1078. https://doi.org/10.1016/j.cell.2017.08.028
Katsoulieris EN, Drossopoulou GI, Kotsopoulou ES et al (2016) High glucose impairs insulin signaling in the glomerulus: an in vitro and ex vivo approach. PLoS One 11:e0158873. https://doi.org/10.1371/journal.pone.0158873
Kaverina I, Stradal TEB, Gimona M (2003) Podosome formation in cultured A7r5 vascular smooth muscle cells requires Arp2/3-dependent de-novo actin polymerization at discrete microdomains. J Cell Sci 116:4915–4924. https://doi.org/10.1242/jcs.00818
Kidani Y, Bensinger SJ (2014) LXR and PPAR as integrators of lipid homeostasis and immunity. J Immunol Rev 249:72–83. https://doi.org/10.1111/j.1600-065X.2012.01153.x.LXR
Kim B, Jo J, Han J et al (2017) In silico re-identification of properties of drug target proteins. BMC Bioinform 18:248. https://doi.org/10.1186/s12859-017-1639-3
Krämer A, Green J, Pollard J, Tugendreich S (2014) Systems biology causal analysis approaches in ingenuity pathway analysis. Bioinformatics 30:523–530. https://doi.org/10.1093/bioinformatics/btt703
Krebs HA (1933) Untersuchungen über den Stoffwechsel der Aminosäuren im Tierkörper. Hoppe-Seyler Z 217:190–227
Kruithof E, Baker M, Bunn C (1995) Biological and clinical aspects of plasminogen activator inhibitor type 2. Blood 86:4006–4024
Krumdieck CL, dos Santos JE, Ho KJ (1980) A new instrument for the rapid preparation of tissue slices. Anal Biochem 104:118–123
Kunst C, Haderer M, Heckel S et al (2016) The p53 family in hepatocellular carcinoma. Transl Cancer Res 5:632–638. https://doi.org/10.21037/11030
Lee SH, Culberson C, Korneszczuk K, Clemens MG (2008) Differential mechanisms of hepatic vascular dysregulation with mild vs. moderate ischemia-reperfusion. Am J Physiol Liver Physiol 294:G1219–G1226. https://doi.org/10.1152/ajpgi.00527.2007
Lee CG, Da Silva CA, Dela Cruz CS et al (2011) Role of chitin and chitinase/chitinase-like proteins in inflammation, tissue remodeling, and injury. Annu Rev Physiol 73:479–501. https://doi.org/10.1146/annurev-physiol-012110-142250
Lemoinne S, Cadoret A, El Mourabit H et al (2013) Origins and functions of liver myofibroblasts. Biochim Biophys Acta Mol Basis Dis 1832:948–954. https://doi.org/10.1016/J.BBADIS.2013.02.019
Li M, de Graaf IAM, Groothuis GMM (2016) Precision-cut intestinal slices: alternative model for drug transport, metabolism, and toxicology research. Expert Opin Drug Metab Toxicol 12:175–190. https://doi.org/10.1517/17425255.2016.1125882
Liu R-M, Gaston Pravia KA (2010) Oxidative stress and glutathione in TGF-β-mediated fibrogenesis. Free Radic Biol Med 48:1–15. https://doi.org/10.1016/j.freeradbiomed.2009.09.026
Lord CC, Thomas G, Brown JM (2013) Mammalian alpha beta hydrolase domain (ABHD) proteins: lipid metabolizing enzymes at the interface of cell signaling and energy metabolism. Biochim Biophys Acta 1831:792–802. https://doi.org/10.1016/j.bbalip.2013.01.002
Luangmonkong T, Suriguga S, Bigaeva E et al (2017) Evaluating the antifibrotic potency of galunisertib in a human ex vivo model of liver fibrosis. Br J Pharmacol 174:3107–3117. https://doi.org/10.1111/bph.13945
Luangmonkong T, Suriguga S, Adhyatmika A et al (2018) In vitro and ex vivo anti-fibrotic effects of LY2109761, a small molecule inhibitor against TGF-β. Toxicol Appl Pharmacol 355:127–137. https://doi.org/10.1016/j.taap.2018.07.001
Lv W, Booz GW, Fan F et al (2018) Oxidative stress and renal fibrosis: recent insights for the development of novel therapeutic strategies. Front Physiol 9:105. https://doi.org/10.3389/fphys.2018.00105
Ma Q (2013) Role of Nrf2 in oxidative stress and toxicity. Annu Rev Pharmacol Toxicol 53:401–426. https://doi.org/10.1146/annurev-pharmtox-011112-140320
MacFie TS, Poulsom R, Parker A et al (2014) DUOX2 and DUOXA2 form the predominant enzyme system capable of producing the reactive oxygen species H_2O_2 in active ulcerative colitis and are modulated by 5-aminosalicylic acid. Inflamm Bowel Dis 20:514–524. https://doi.org/10.1097/01.MIB.0000442012.45038.0e
Mann J, Chu DCK, Maxwell A et al (2010) MeCP2 controls an epigenetic pathway that promotes myofibroblast transdifferentiation and fibrosis. Gastroenterology 138:705–714.e4. https://doi.org/10.1053/j.gastro.2009.10.002

Marcovina SM, Sirtori C, Peracino A et al (2013) Translating the basic knowledge of mitochondrial functions to metabolic therapy: role of L-carnitine. Transl Res 161:73–84. https://doi.org/10.1016/j.trsl.2012.10.006

Mathema VB, Koh Y-S, Thakuri BC, Sillanpää M (2012) Parthenolide, a sesquiterpene lactone, expresses multiple anti-cancer and anti-inflammatory activities. Inflammation 35:560–565. https://doi.org/10.1007/s10753-011-9346-0

Medcalf RL, Stasinopoulos SJ (2005) The undecided serpin. The ins and outs of plasminogen activator inhibitor type 2. FEBS J 272:4858–4867. https://doi.org/10.1111/j.1742-4658.2005.04879.x

Meng X, Nikolic-Paterson DJ, Lan HY (2016) TGF-β: the master regulator of fibrosis. Nat Rev Nephrol 12:325–338. https://doi.org/10.1038/nrneph.2016.48

Metzker ML (2010) Sequencing technologies—the next generation. Nat Rev Genet 11:31–46. https://doi.org/10.1038/nrg2626

Mimche PN, Lee CM, Mimche SM et al (2018) EphB2 receptor tyrosine kinase promotes hepatic fibrogenesis in mice via activation of hepatic stellate cells. Sci Rep 8:2532. https://doi.org/10.1038/s41598-018-20926-9

Murthy S, Born E, Mathur SN, Field FJ (2002) LXR/RXR activation enhances basolateral efflux of cholesterol in CaCo-2 cells. J Lipid Res 43:1054–1064. https://doi.org/10.1194/jlr.M100358-JLR200

Orsucci D, Mancuso M, Ienco EC et al (2011) Targeting mitochondrial dysfunction and neurodegeneration by means of coenzyme Q10 and its analogues. Curr Med Chem 18:4053–4064. https://doi.org/10.2174/092986711796957257

Osman G, Rodriguez J, Chan SY et al (2018) PEGylated enhanced cell penetrating peptide nanoparticles for lung gene therapy. J Control Release 285:35–45. https://doi.org/10.1016/j.jconrel.2018.07.001

Overall CM (2002) Molecular determinants of metalloproteinase substrate specificity: matrix metalloproteinase substrate binding domains, modules, and exosites. Mol Biotechnol 22:051–086. https://doi.org/10.1385/MB:22:1:051

Page-McCaw A, Ewald AJ, Werb Z (2007) Matrix metalloproteinases and the regulation of tissue remodelling. Nat Rev Mol Cell Biol 8:221–233. https://doi.org/10.1038/nrm2125

Parajuli N, Doppler W (2009) Precision-cut slice cultures of tumors from MMTV-neu mice for the study of the ex vivo response to cytokines and cytotoxic drugs. Vitr Cell Dev Biol Anim 45:442–450. https://doi.org/10.1007/s11626-009-9212-7

Parks WC, Wilson CL, López-Boado YS (2004) Matrix metalloproteinases as modulators of inflammation and innate immunity. Nat Rev Immunol 4:617–629. https://doi.org/10.1038/nri1418

Pham BT, van Haaften WT, Oosterhuis D et al (2015) Precision-cut rat, mouse, and human intestinal slices as novel models for the early-onset of intestinal fibrosis. Physiol Rep 3:e12323. https://doi.org/10.1414/phy2.12323

Piccinini AM, Midwood KS (2010) DAMPening inflammation by modulating TLR signalling. Mediat Inflamm 2010:1–21. https://doi.org/10.1155/2010/672395

Poli G (2000) Pathogenesis of liver fibrosis: role of oxidative stress. Mol Aspects Med 21:49–98

Ratziu V, Harrison SA, Francque S et al (2016) Elafibranor, an agonist of the peroxisome proliferator– activated receptor– α and– δ, induces resolution of nonalcoholic steatohepatitis without fibrosis worsening. Gastroenterology 150:1147–1159.e5. https://doi.org/10.1053/j.gastro.2016.01.038

Rehli M, Niller H-H, Ammon C et al (2003) Transcriptional regulation of CHI3L1, a marker gene for late stages of macrophage differentiation. J Biol Chem 278:44058–44067. https://doi.org/10.1074/jbc.M306792200

Remst DFG, Blaney Davidson EN, van der Kraan PM (2015) Unravelling osteoarthritis-related synovial fibrosis: a step closer to solving joint stiffness. Rheumatology 54:1954–1963. https://doi.org/10.1093/rheumatology/kev228

Rieder F, Brenmoehl J, Leeb S et al (2007) Wound healing and fibrosis in intestinal disease. Gut 56:130–139. https://doi.org/10.1136/gut.2006.090456

Rockey DC, Bell PD, Hill JA (2015) Fibrosis—a common pathway to organ injury and failure. N Engl J Med 372:1138–1149. https://doi.org/10.1056/NEJMra1300575

Roduit R, Morin J, Massé F et al (2000) Glucose down-regulates the expression of the peroxisome proliferator-activated receptor-α gene in the pancreatic β-cell. J Biol Chem 275:35799–35806. https://doi.org/10.1074/jbc.M006001200

Ruigrok MJR, Maggan N, Willaert D et al (2017) siRNA-mediated RNA interference in precision-cut tissue slices prepared from mouse lung and kidney. AAPS J 19:1855–1863. https://doi.org/10.1208/s12248-017-0136-y

Sack GH Jr (2018) Serum amyloid A—a review. Mol Med 24:46. https://doi.org/10.1186/s10020-018-0047-0

Sahin H, Wasmuth HE (2013) Chemokines in tissue fibrosis. Biochim Biophys Acta Mol Basis Dis 1832:1041–1048. https://doi.org/10.1016/j.bbadis.2012.11.004

Sato Y, Yanagita M (2017) Resident fibroblasts in the kidney: a major driver of fibrosis and inflammation. Inflamm Regen 37:17. https://doi.org/10.1186/s41232-017-0048-3

Schafer S, Viswanathan S, Widjaja AA et al (2017) IL-11 is a crucial determinant of cardiovascular fibrosis. Nature 552:110–115. https://doi.org/10.1038/nature24676

Schwertschlag US, Trepicchio WL, Dykstra KH et al (1999) Hematopoietic, immunomodulatory and epithelial effects of interleukin-11. Leukemia 13:1307–1315

Shay KP, Moreau RF, Smith EJ et al (2009) Alpha-lipoic acid as a dietary supplement: molecular mechanisms and therapeutic potential. Biochim Biophys Acta 1790:1149–1160. https://doi.org/10.1016/j.bbagen.2009.07.026

Sims GP, Rowe DC, Rietdijk ST et al (2010) HMGB1 and RAGE in inflammation and cancer. Annu Rev Immunol 28:367–388. https://doi.org/10.1146/annurev.immunol.021908.132603

Söllner JF, Leparc G, Hildebrandt T et al (2017) Data descriptor: an RNA-Seq atlas of gene expression in mouse and rat normal tissues background and summary. Nat Publ Gr. https://doi.org/10.1038/sdata.2017.185

Speca S (2012) Cellular and molecular mechanisms of intestinal fibrosis. World J Gastroenterol 18:3635. https://doi.org/10.3748/wjg.v18.i28.3635

Stribos EGD, Luangmonkong T, Leliveld AM et al (2016) Precision-cut human kidney slices as a model to elucidate the process of renal fibrosis. Transl Res 170:8–16.e1. https://doi.org/10.1016/j.trsl.2015.11.007

Stribos EGD, Seelen MA, van Goor H et al (2017) Murine precision-cut kidney slices as an ex vivo model to evaluate the role of transforming growth factor-β1 signaling in the onset of renal fibrosis. Front Physiol 8:1026. https://doi.org/10.3389/fphys.2017.01026

't Hart NA, van der Plaats A, Faber A et al (2005) Oxygenation during hypothermic rat liver preservation: an in vitro slice study to demonstrate beneficial or toxic oxygenation effects. Liver Transplant 11:1403–1411. https://doi.org/10.1002/lt.20510

Trapnell C, Hendrickson DG, Sauvageau M et al (2013) Differential analysis of gene regulation at transcript resolution with RNA-seq. Nat Biotechnol 31:46–53. https://doi.org/10.1038/nbt.2450

Tschumperlin DJ (2013) Fibroblasts and the ground they walk on. Physiology 28:380–390. https://doi.org/10.1152/physiol.00024.2013

Vatakuti S, Pennings JLA, Gore E et al (2016) Classification of cholestatic and necrotic hepatotoxicants using transcriptomics on human precision-cut liver slices. Chem Res Toxicol 29:342–351. https://doi.org/10.1021/acs.chemrestox.5b00491

Wajner M, Amaral AU (2016) Mitochondrial dysfunction in fatty acid oxidation disorders: insights from human and animal studies. Biosci Rep 36:e00281. https://doi.org/10.1042/BSR20150240

Warburg O (1923) Versuche an überlebendem karzinomgewebe. Biochem Z 142:317–333

Westra IM, Pham BT, Groothuis GMM, Olinga P (2013) Evaluation of fibrosis in precision-cut tissue slices. Xenobiotica 43:98–112. https://doi.org/10.3109/00498254.2012.723151

Westra IM, Oosterhuis D, Groothuis GMM, Olinga P (2014) Precision-cut liver slices as a model for the early onset of liver fibrosis to test antifibrotic drugs. Toxicol Appl Pharmacol 274:328–338. https://doi.org/10.1016/j.taap.2013.11.017

Westra IM, Mutsaers HAM, Luangmonkong T et al (2016) Human precision-cut liver slices as a model to test antifibrotic drugs in the early onset of liver fibrosis. Toxicol Vitro 35:77–85. https://doi.org/10.1016/j.tiv.2016.05.012

Wohlsen A, Uhlig S, Martin C (2001) Immediate allergic response in small airways. Am J Respir Crit Care Med 163:1462–1469. https://doi.org/10.1164/ajrccm.163.6.2007138

Wynn T (2004) Fibrotic disease and the TH1/TH2 paradigm. Nat Rev Immunol 4:583–594. https://doi.org/10.1038/nri1412

Wynn T (2008) Cellular and molecular mechanisms of fibrosis. J Pathol 214:199–210. https://doi.org/10.1002/path.2277

Yadav NK, Shukla P, Omer A et al (2014) Next generation sequencing: potential and application in drug discovery. Sci World J 2014:1–7. https://doi.org/10.1155/2014/802437

Yamaguchi H, Lorenz M, Kempiak S et al (2005) Molecular mechanisms of invadopodium formation. J Cell Biol 168:441–452. https://doi.org/10.1083/jcb.200407076

Yu R, Jiang S, Tao Y et al (2019) Inhibition of HMGB1 improves necrotizing enterocolitis by inhibiting NLRP3 via TLR4 and NF-κB signaling pathways. J Cell Physiol 234:13431–13438. https://doi.org/10.1002/jcp.28022

Zeisberg M, Kalluri R (2013) Cellular mechanisms of tissue fibrosis. 1. common and organ-specific mechanisms associated with tissue fibrosis. Am J Physiol Physiol 304:C216–C225. https://doi.org/10.1152/ajpcell.00328.2012

Zhang Q, Raoof M, Chen Y et al (2010) Circulating mitochondrial DAMPs cause inflammatory responses to injury. Nature 464:104–107. https://doi.org/10.1038/nature08780

Zhong T, Tang J, Liu Y et al (2009) High mobility group box-1 stimulates proinflammatory cytokine production in endothelial cells via MAP kinases. Nan Fang Yi Ke Da Xue Xue Bao 29:1517–1520

Affiliations

Emilia Bigaeva[1] · Emilia Gore[1] · Eric Simon[2] · Matthias Zwick[2] · Anouk Oldenburger[3] · Koert P. de Jong[4] · Hendrik S. Hofker[5] · Marco Schlepütz[6] · Paul Nicklin[7] · Miriam Boersema[1] · Jörg F. Rippmann[3] · Peter Olinga[1]

1 Department of Pharmaceutical Technology and Biopharmacy, University of Groningen, Antonius Deusinglaan 1, Groningen 9713AV, The Netherlands

2 Computational Biology, Boehringer Ingelheim Pharma GmbH & Co. KG, Birkendorfer Str. 65, 88397 Biberach an der Riss, Germany

3 Cardiometabolic Disease Research, Boehringer Ingelheim Pharma GmbH & Co. KG, Birkendorfer Str. 65, 88397 Biberach an der Riss, Germany

4 Department of Hepato-Pancreato-Biliary Surgery and Liver Transplantation, University Medical Center Groningen, University of Groningen, Hanzeplein 1, 9713 GZ Groningen, The Netherlands

5 Department of Surgery, University Medical Center Groningen, University of Groningen, Hanzeplein 1, 9713 GZ Groningen, The Netherlands

6 Respiratory Diseases, Boehringer Ingelheim Pharma GmbH & Co. KG, Birkendorfer Str. 65, 88397 Biberach an der Riss, Germany

7 Research Beyond Borders, Boehringer Ingelheim Pharma GmbH & Co. KG, Birkendorfer Str. 65, 88397 Biberach an der Riss, Germany